



**NASA  
Technical  
Paper  
3354**

November 1993

---

# Calculations of Cosmic-Ray Helium Transport in Shielding Materials

Francis A. Cucinotta

  
**NASA  
Technical  
Paper  
3354**

1993

---

# Calculations of Cosmic-Ray Helium Transport in Shielding Materials

Francis A. Cucinotta  
*Langley Research Center  
Hampton, Virginia*

## Symbols

$A$	mass number
$A_P$	mass number of projectile
$A_T$	mass number of target
$\mathbf{b}$	impact parameter
$B$	slope parameter, fm <sup>2</sup>
$C_F$	fragment downshift, MeV/amu
$c$	speed of light fm/s
$D$	dose, cGy
$d$	<sup>2</sup> H
$E$	particle energy, MeV/amu
$E'$	$= \varepsilon(\tau')$
$E_a$	energy of cluster $a$
$E_m$	maximum kinetic energy of fragment, MeV/amu
$E_0$	beam kinetic energy, MeV/amu
$E_{0j}$	average energy of target fragment $j$
$E_{th}$	threshold energy, MeV
$F$	defined in equation (12)
$\overline{F}$	defined in equation (11)
$\bar{f}$	scaled spectrum, mb/(g/cm <sup>2</sup> )
$f_{jk}(E, E')$	differential energy cross section for redistribution of particle type and energy
$G_0$	Green's function, MeV <sup>-1</sup>
$H$	dose equivalent, cSv
$h$	<sup>3</sup> He
$K$	relative wave number, fm <sup>-1</sup>
$m$	number of target knockouts
$m_N$	nucleon mass, MeV/ $c^2$
$N$	number of energy grid points
$N_F$	normalization constant
$n$	neutron
$P$	projectile
$PF$	projectile fragment
$p$	proton
$\mathbf{p}$	momentum, MeV/ $c$
$Q$	binding energy difference, MeV

$\mathbf{q}$	momentum transfer vector, $\text{fm}^{-1}$
$R$	nuclear matter radii, fm
$R_T$	matter radii of target, fm
$R_\alpha$	matter radii of alpha particle, fm
$r$	residual range, $\text{g}/\text{cm}^2$
$\sqrt{S}$	total energy in three-body center-of-mass frame, MeV
$S(E)$	proton stopping power, $\text{MeV}/(\text{g}/\text{cm}^2)$
$T$	target
$TF$	target fragment
$\hat{T}_{aT}, \hat{T}_{bT}, \hat{T}_{ab}$	two-body amplitudes, MeV
$T_{\text{lab}}$	initial energy, $\text{MeV}/\text{amu}$
$t$	${}^3\text{H}$
$W_F$	width, $\text{MeV}/\text{amu}$
$W_m$	collision terms to $m$ th order inelastic scattering
$X$	final target state
$x$	depth of material, $\text{g}/\text{cm}^2$
$Z$	charge
$z$	distance, $\text{g}/\text{cm}^2$
$\alpha$	alpha particle
$\beta$	relative projectile-target velocity
$\gamma(a, x)$	incomplete gamma function
$\delta$	Dirac delta function
$\epsilon_B$	binding energy of projectile clusters, MeV
$\epsilon(r)$	energy associated with residual range $r$ , $\text{MeV}/\text{amu}$
$\zeta_j(r, t)$	defined by equation (7)
$\eta$	defined by equation (29)
$\theta$	unit step function
$\theta_{\text{lab}}$	scattering angle in lab system
$\nu_j$	range scaling parameter
$\sigma$	cross section, mb
$\sigma_{\text{abs}}$	absorption cross section, mb
$\sigma_F$	fragmentation cross section, mb
$\sigma_j(E)$	total cross section, mb
$\sigma_{\text{pickup}}$	pickup cross section, mb
$\hat{\tau}$	transition operator, MeV
$\tau_{fi}$	transition matrix, MeV

$\Phi$	error function
$\phi_j(x, E)$	differential flux spectrum of type $j$ ions
$\chi$	mean distorting wave
$\Psi_j$	scaled flux
$\Omega$	solid angle
$\omega$	energy loss of projectile fragment, MeV/amu
Subscripts:	
$f$	final state
$i$	initial state
$j, k$	ions of type $j$ and $k$
$M$	maximum
$QE$	quasi-elastic

## Abstract

*The transport of galactic cosmic-ray helium nuclei and their secondaries through bulk shielding is considered using the straight-ahead approximation to the Boltzmann equation. A data base for nuclear interaction cross sections and secondary particle energy spectra for high-energy light-ion breakup is presented. The importance of the light ions  $^2\text{H}$ ,  $^3\text{H}$ , and  $^3\text{He}$  for cosmic-ray risk estimation is discussed, and the estimates of the fractional contribution to the neutron flux from helium interactions compared with other particle interactions are presented using a 1977 solar minimum cosmic-ray spectrum.*

## Introduction

The description of the transport of solar and cosmic radiation in spacecraft and satellites is important for estimating radiation biological harm to astronauts. The galactic cosmic rays (GCR's) contain a large alpha-particle component that consists of approximately 10 percent of the total flux; this alpha-particle component is second in size only to the hydrogen component (ref. 1). Light-ion transport will be important for studying the large solar particle events that contain a significant alpha-particle component in addition to the dominant protons (refs. 2 and 3). Target fragmentation effects also produce a large fluence of alpha particles and other light ions; these particles and ions are expected to be biologically damaging because their spectra peak at low energies. An accurate physical description of the transport alpha particles is thus needed for estimating the radiation fields to be encountered by astronauts in spaceflight. The production of  $^2\text{H}$  and  $^3\text{He}$  from alpha-particle fragmentation is also useful to estimate the natural abundance of these elements in the GCR's.

For high-energy, charged-particle transport, the straight-ahead approximation is accurate. The solution of the Boltzmann equation for particle propagation in shielding materials has been developed by Wilson and Lamkin (ref. 4) and Wilson (ref. 5), and a space radiation transport code called BRYNTRN (refs. 6 and 7) provides an accurate numerical procedure. The accuracy of the solution is also dependent on the nuclear interaction cross sections for fragmentation reactions in shielding materials (ref. 8). Presently, there is a scarcity of experimental measurements for fragmentation cross sections; therefore, theoretical models must be used to provide the large data base of cross sections for transport in spacecraft shielding and tissue. One approximation made for heavy projectile fragments is that the secondary spectrum is a delta function corresponding to the beam velocity that closely resembles experimental observation; however, for light secondaries, the spectrum is much broader. This broader spectrum places an extra burden on the development of a data base because the secondary spectrum, as well as the total yield of each species, must be represented in the code.

In this paper, we discuss the development of a parametric data base for alpha-particle interactions and secondaries  $^3\text{He}$  ( $h$ ),  $^3\text{H}$  ( $t$ ), and  $^2\text{H}$  ( $d$ ) in arbitrary materials based on theoretical models and limited experimental information. A description of the extension of the BRYNTRN code for light-ion transport is also described, and predictions for cosmic-ray helium transport are discussed. Alpha particles will be the dominant source of high-energy neutrons ( $>100$  MeV) in the GCR's and an important source of low-energy neutrons. Estimates of the fractional contribution of secondary neutrons compared with neutron production from other particle types will also be discussed. Light-ion secondaries from target fragmentation are included in the transport equations. In previous treatments (refs. 6 and 7), these secondaries were included as a local source. The new procedure has the advantage of including the effects of any further nuclear reactions and their contributions to the linear energy transfer spectrum.

## Transport Equations and Solutions

The propagation of high-energy  $^4\text{He}$  and its secondaries through bulk matter is described by the Boltzmann equation, which in the straight-ahead approximation is of the following form (refs. 5 and 6):

$$\left[ \frac{\partial}{\partial x} - \nu_j \frac{\partial}{\partial E} S(E) + \sigma_j(E) \right] \phi_j(x, E) = \sum_k \int_0^\infty f_{jk}(E, E') \phi_k(x, E') dE' \quad (1)$$

where  $\nu_j$  (which denotes the range scaling parameter) is equal to  $Z_j^2/A_j$ . The terms  $Z$  and  $A$  are the charge and the mass number, respectively. In equation (1),  $S(E)$  is the proton stopping power,  $\sigma_j(E)$  is the total cross section,  $\phi_j(x, E)$  is the differential flux spectrum of type  $j$  ions, and  $f_{jk}(E, E')$  is a differential energy cross section for the redistribution of particle type and energy.

Utilizing the definitions

$$r = \int_0^E \frac{dE'}{S(E')} \quad (2)$$

$$\Psi_j(x, r) = S(E') \phi_j(x, E) \quad (3)$$

and

$$\bar{f}_{jk}(r, r') = S(E') f_{jk}(E, E') \quad (4)$$

allows equation (1) to be rewritten as

$$\left[ \frac{\partial}{\partial x} - \nu_j \frac{\partial}{\partial r} + \sigma_j(r) \right] \Psi_j(x, r) = \sum_k \int_r^\infty \bar{f}_{jk}(r, r') \Psi_k(x, r') dr' \quad (5)$$

This equation is solved by Wilson (ref. 5) and Wilson et al. (ref. 6) as

$$\Psi_j(x, r) = \exp[-\zeta_j(r, x)] \Psi_j(0, r + \nu_j x) + \sum_k \int_0^x \int_r^\infty \exp[-\zeta_j(r, x)] \bar{f}_{jk}(r + \nu_j z, r') \Psi_k(x - z, r') dr' dz \quad (6)$$

where the exponential quantity is the integrating factor given by

$$\zeta_j(r, t) = \int_0^t \sigma_j(r + \nu_j t') dt' \quad (7)$$

Equation (7) is the basis of the numerical procedures for propagation of the solution at  $\Psi_j(x, r)$  to  $\Psi_j(x + h, r)$ . If we choose  $h$  to be small such that

$$\sigma_j(r') h \ll 1 \quad (8)$$

the solution at  $x + h$  (ref. 6) is approximately

$$\begin{aligned} \Psi_j(x + h, r) &\cong \exp[-\zeta_j(r, h)] \Psi_j(x_j, r + \nu_j h) \\ &+ \sum_k \exp \left\{ - \left[ \zeta_j \left( r, \frac{h}{2} \right) + \zeta_k \left( r, \frac{h}{2} \right) \right] \right\} \bar{F} \left( r, \nu_j h, r_k + \frac{\nu_j h}{2} \right) \\ &\times \int_{r_{k+(\nu_j h/2)+(\nu_k h/2)}}^{r_k} \Psi_k(x, r') dr' \end{aligned} \quad (9)$$

for charged-particle propagation and

$$\begin{aligned} \Psi_n(x+h, r) &\cong \exp[-\zeta_n(r, h)] \Psi_n(x, r) \\ &+ \sum_k \int_r^\infty \exp \left\{ - \left[ \zeta_n \left( r, \frac{h}{2} \right) + \zeta_k \left( r', \frac{h}{2} \right) \right] \right\} \\ &\times f_{jk}(r, r') \Psi_k \left( x, r' + \nu_k \frac{h}{2} \right) dr' \end{aligned} \quad (10)$$

for neutron propagation. In equation (9),  $\bar{F}$  is related to the cumulative spectrum  $F$  as

$$\bar{F}_{ij}(h, r, r') = \int_0^h \bar{f}_{ij}(r+z, r') dz \equiv F_{ij}(r+h, r') - F_{ij}(r, r') \quad (11)$$

with

$$F_{ij}(r, r') = \int_0^{\varepsilon(r)} f_{ij}(E, E') dE \quad (12)$$

where  $\varepsilon(r)$  is the energy associated with the residual range  $r$  and  $E' = \varepsilon(r')$ . The numerical procedures for evaluating equations (6) to (12) have been described in references 6 and 9.

For nuclear secondaries produced from target nuclei with  $A > 4$ , the probabilities for nuclear collisions are small because these will be low-energy ions (e.g., typically only a few MeV). The differential flux for these ions can then be solved in closed form for the target fragments with  $A > 4$  as

$$\phi_j(x, E) = \frac{1}{S_j(E)} \sum_k \int_E^\infty f_{kj}(E, E') \phi_k(x, E) dE' \quad (13)$$

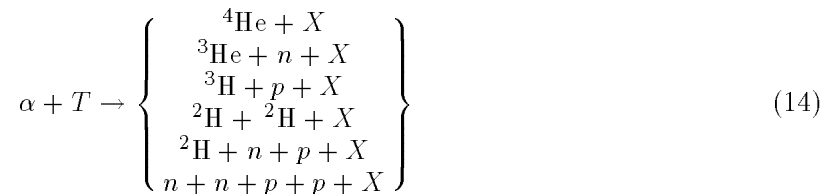
The light-ion target fragments have been treated in the past (refs. 6 and 7) by using equation (13); however, here they will be included in the transport solutions.

Reference 6 describes the numerical representation of particle ranges and stopping powers in the BRYNTRN code. For energies greater than a few MeV/amu, Bethe's theory using the Born approximation is adequate if the appropriate corrections to Bragg's rule, the shell corrections, and the effective charge are included. Proton stopping powers are taken from the parametric expressions of Andersen and Ziegler (ref. 10). A modification to their shell corrections, however, has been added to ensure a smooth transition to Bethe's asymptotic formula. For alpha particles, the electronic stopping power cannot be derived from the proton stopping power at low energies because of the neglect of higher order Born terms. Instead, we use Ziegler's method (refs. 11 and 12) based on fits to the experimental data. For low energies, the nuclear stopping theory used herein is a modified form of the theory of Lindhard et al. (ref. 13).

## Light Ion Fragmentation on Nuclear Targets

Although the alpha particle is the most compact and tightly bound nucleus, this does not preclude its breakup in the field of target nuclei. Fragmentation of cosmic-ray alpha particles may lead to an important source of high-energy neutrons that will have large ranges and high values for relative biological effectiveness. Theoretical models of light-ion cross sections have been developed (refs. 14 to 20), and we now consider these models for providing a data base.

The fragmentation of  $^4\text{He}$  is simpler than that of a heavier nucleus because only a small number of final states can occur. These reactions are



where  $T$  is the target and  $X$  is the final target. Each of the reactions in equation (14) can occur with or without meson production if sufficient energy is available. The reactions in equation (14) are not exhaustive of the absorption processes; most notable of these reactions are the compound nuclear and pickup channels that are important at low energies. A model for the two-body dissociation of light ions has been developed (refs. 16, 17, and 20), and this model describes the first three reactions in equation (14), which we now discuss. The fragmentation of the composite secondaries of  ${}^4\text{He}$  ( ${}^2\text{H}$ ,  ${}^3\text{H}$ , or  ${}^3\text{He}$ ) is described by the same model.

For an inclusive reaction involving the two-body dissociation of the projectile  $P$ , we write

$$P + T \rightarrow a + b + X \quad (15)$$

where  $a$  and  $b$  are assumed to be the clusters that are initially present in the projectile and  $X$  is the final unobserved target state. We consider the case in which  $a$  is the observed projectile fragment in the measurement. Note that we must sum the unobserved target states to evaluate the cross section. We should also consider summing possible states of the particle  $b$ . Using relativistic kinematics, the transition matrix for equation (15) is related to the Lorentz invariant momentum distribution for producing the fragment  $a$  by

$$E_a \frac{d\sigma}{d\mathbf{p}_a} = E_a \frac{(2\pi)^4}{\beta} \int d\mathbf{p}_b \sum_{m=1}^{A_T} \prod_{j=1}^m d\mathbf{p}_j \delta(\mathbf{p}_f - \mathbf{p}_i) \delta(E_f - E_i) |\tau_{fi}|^2 \quad (16)$$

where  $f$  and  $i$  label the final and initial states,  $\beta$  is the relative projectile-target velocity, and  $\tau_{fi}$  is the transition matrix. The summation in equation (16) is over the possible configurations of the target in the final state.

The transition matrix can be written as a three-body problem of  $aT$ ,  $bT$ , and  $ab$  interactions when rearrangement channels are neglected and with the understanding that all target final and intermediate states must be summed. Using the Faddeev method, we consider the multiple-scattering series generated by the coupled set of integral equations

$$\hat{\tau} = \hat{\tau}^a + \hat{\tau}^b + \hat{\tau}^T \quad (17)$$

with

$$\hat{\tau}^a = \hat{T}_{bT} + \hat{T}_{bT} G_0 (\hat{\tau}^b + \hat{\tau}^T) \quad (18)$$

$$\hat{\tau}^b = \hat{T}_{aT} + \hat{T}_{aT} G_0 (\hat{\tau}^a + \hat{\tau}^T) \quad (19)$$

$$\hat{\tau}^T = \hat{T}_{ab} + \hat{T}_{ab} G_0 (\hat{\tau}^a + \hat{\tau}^b) \quad (20)$$

where  $\hat{T}_{aT}$ ,  $\hat{T}_{bT}$ , and  $\hat{T}_{ab}$  are the ‘‘two-body’’ amplitudes that are the transition operators for  $aT$ ,  $bT$ , or  $ab$  scattering, respectively, in the projectile-target Hilbert space. Solutions for the amplitudes related to  $\hat{T}_{aT}$  and  $\hat{T}_{bT}$  are found (refs. 15 and 19) from Watson’s multiple-scattering series in the eikonal approximation. The amplitude related to  $\hat{T}_{ab}$  will only be important at small  $ab$  relative momentum, and it is evaluated in a separable potential model. The Green’s function  $G_0$  is evaluated in the impulse approximation that neglects the binding of the nuclei of  $a$ ,  $b$ , and  $T$  with respect to their kinetic energies.

We consider the leading terms of equation (17) by truncating as

$$\hat{\tau} \cong \left(1 + \hat{T}_{ab} G_0\right) \left(\hat{T}_{aT} + \hat{T}_{bT} + \hat{T}_{aT} G_0 \hat{T}_{bT} + \hat{T}_{bT} G_0 \hat{T}_{aT}\right) \quad (21)$$

which considers the scattering to all orders but neglects reflection terms between projectile and target nucleons. This equation assumes that the final-state interaction (FSI) between projectile fragments occurs only after interactions with the target.

The evaluation of the momentum distribution, equation (16), using equation (21), proceeds after an introduction of the vertex functions for the projectile decay and the inclusive scattering distributions for  $a$  or  $b$  interacting on the target. The vertex function is parameterized as a sum of Yukawa functions with the proper asymptotic behavior at large  $ab$  separation distances. Reference 20 gives the values for parameters of the Yukawa representation of the vertex functions for light ions.

The inclusive scattering distributions for  $a$  or  $b$  reacting on the target are found (refs. 18 and 19) as

$$\left( \frac{d^2\sigma}{d\Omega dE} \right) = \frac{K^2}{(2\pi)^2} \int d^2b d^2b' \exp[i\mathbf{q}(\mathbf{b} - \mathbf{b}')] \exp\{i[\chi(\mathbf{b}) - \chi^\dagger(\mathbf{b}')]\} \sum_{m=1}^{A_T} W_m(\mathbf{b}, \mathbf{b}', \omega) \quad (22)$$

where  $K$  is the relative wave number,  $\chi$  is a mean distorting wave in the eikonal approximation,  $\mathbf{q}$  is the momentum transfer,  $\omega$  is the energy loss of the projectile fragment, and  $W_m$  are the collision terms for the  $m$ th order inelastic scattering. The collision terms are related to the two-body amplitudes, and the form factors of the projectile cluster ( $a$  or  $b$ ) and the ground-state response functions (Green's functions) of the target (refs. 18 and 19). The elastic fragmentation terms are included using a first-order optical model solution for the  $aT$  or  $bT$  amplitude. The on-shell spectra represented by equation (22) are used to approximate the off-shell amplitudes  $\hat{T}_{aT}$  in equation (21). Figures 1 and 2 show the calculations of total  $\alpha$ -nucleus reactions as a function of the invariant momentum transfer for several targets compared with the data of reference 21. Calculations of the inelastic part are from equation (22) after integrating the energy loss. The elastic part is calculated in the first-order optical model. The results indicate the accuracy of using equation (22) for inclusive scattering at high energies.

Figure 3 shows the angular distribution for  ${}^3\text{He}$  production in  $\alpha + {}^1\text{H}$  reactions at 1.04 GeV compared with the data of reference 22. The calculations show an important interference effect among the terms in equation (21). Figure 4 shows the calculations of the invariant momentum distribution in the longitudinal direction near 2.0 GeV incident energy with data from reference 23, and figure 5 gives data from references 24 and 25 for the transverse direction. Theoretical calculations provide a good representation of the data and indicate the importance of final-state interactions. Results at other energies as described in reference 20 indicate a similar success for the light-ion breakup model just described.

The spectral distributions of secondaries used for the solution of the Boltzmann equation (5) are obtained from equation (14) after integrating the solid angle. Total fragmentation cross sections are obtained from equation (14) after integrating both the solid angle and the momentum of the fragment. Table 1 presents the results of calculations for  ${}^3\text{H}$  and  ${}^3\text{He}$  production compared with experimental data (refs. 22, 26, and 27).

## Parameterizations of Interaction Cross Sections

We next discuss parameterizations of interaction cross sections for light ions in common shielding materials. The work of Meyer (ref. 26) gives a complete summary of  $\alpha$ - ${}^1\text{H}$  cross sections based on measurements taken until 1972. Parameterizations of  ${}^3\text{H}$  and  ${}^3\text{He}$  production of  ${}^1\text{H}$  below 300 MeV/amu are discussed in reference 28. An extensive list of earlier references of experiments is given in reference 26. Reference 29 discusses more recent experiments in absorption cross sections between 18 and 48 MeV. Reference 30 describes deuteron production at 1.4 GeV/amu which was measured with the inclusive deuteron production cross section reported at  $30.64 \pm 0.62$  mb. The results for the  $A = 3$  fragments are given in references 22 and 27, and these results postdate the compilation by Meyer. The most important shortcomings of the data base for  ${}^4\text{He}$ - ${}^1\text{H}$  interactions are high-energy measurements above a few GeV and a complete absence of data for nucleon production cross sections.

Using our theoretical estimates and the existing data, we parameterize the fragmentation cross sections for  ${}^3\text{He}$ ,  ${}^3\text{H}$ , and  ${}^2\text{H}$  production of  ${}^1\text{H}$  as

$$\begin{aligned} \sigma_{{}^3\text{He}} &= 42.5 \left[ \frac{2}{1 + \exp[(E_{th} - E)/6.8]} - 1 \right] \\ &\times \left[ 1 - \frac{0.51}{1 + 6.7 \exp(-E/34)} \right]^3 \left( 1 + 0.36 \sqrt{\frac{E}{520}} \right) \exp[-(E - 780)/2300] \end{aligned} \quad (23)$$

$$\begin{aligned} \sigma_{{}^3\text{H}} &= 15.5 \left[ \frac{2}{1 + \exp[(E_{th} - E)/7]} - 1 \right] \\ &\times \left[ 1 - \frac{0.45}{1 + 7 \exp(-E/55)} \right]^3 \left( 1 + 1.8 \sqrt{\frac{E}{550}} \right) \exp[-(E - 750)/4500] \end{aligned} \quad (24)$$

and

$$\sigma_d = 17 \left[ \frac{2}{1 + \exp[(E_{th} - E)/12]} - 1 \right] \times \left\{ 1 - \frac{0.21(E/145 - 1)}{1 + \exp[(145 - E)/6]} \right\} \exp(-E/3000) \quad (25)$$

where  $E_{th}$  is the threshold energy for the breakup reaction listed in table 2 (ref. 31), and  $E$  is the kinetic energy in units of MeV/amu. The low-energy behavior of equation (25) resembles that of the behavior in reference 28. The pickup cross section  $\sigma_{\text{pickup}}$  is parameterized as

$$\sigma_{\text{pickup}} = 48 \exp[-(E - E_{th})^{1.7/3000}] \quad (26)$$

and contributes to the inclusive  ${}^3\text{He}$  and  ${}^2\text{H}$  production cross sections. At low energies, the resonance  ${}^5\text{Li}$  (which is not considered here) occurs. Figures 6 to 8 compare parameterizations with experimental data. All cross sections are set constant above 3 GeV/amu. The energy variations near the thresholds and the pion production region are accurately reproduced. For the  ${}^1\text{H}$  target, the absorption cross section  $\sigma_{\text{abs}}$  below 80 MeV is assumed as

$$\sigma_{\text{abs}} = \sigma_{{}^3\text{He}} + \sigma_{{}^3\text{H}} + \sigma_{{}^2\text{H}} + \sigma_{\text{pickup}} \quad (27)$$

Above 80 MeV (and below 80 MeV for  $A_T > 1$ ), we use the energy-dependent parameterization of Townsend and Wilson (ref. 32).

$$\sigma_{\text{abs}} = 10\pi\beta(E) \left[ R_{4\text{He}} + R_{A_T} - 1.26\eta(E) \right]^2 \quad (28)$$

where

$$\begin{aligned} \beta(E) &= 1 + \frac{5}{T} \\ \eta(E) &= 0.2 + \frac{1}{A_P} + \frac{1}{A_T} - 0.292 \exp(-E/792) \cos\left(0.228E^{0.453}\right) \end{aligned} \quad (29)$$

with a normalization correction of 0.95 used for  ${}^1\text{H}$ . The argument of the cosine function is in radians. In equation 28, the nuclear matter radii  $R$  are used. Figure 9 shows the absorption cross section for  $\alpha$ - ${}^1\text{H}$ . An excellent reproduction of the experimental data is seen.

The proton and the neutron productions are expected to rise dramatically above pion production thresholds because two-body collisions will be predominantly inelastic, thus leading to pion

absorption in the  $A = 3$  or  $A = 2$  clusters. Pion production has not been treated in our theoretical considerations. However, the expected rise in proton and neutron cross sections occurs if we simply balance the absorption cross section with channels that do not lead to proton and neutron production, respectively. Figure 10 presents these results.

The experimental data base for composite targets is extremely small. Figure 11 shows a comparison of equation (28) with data for the  ${}^4\text{He} + {}^{12}\text{C}$  absorption cross sections. Agreement is excellent, and a previous analysis (ref. 32) suggests that a similar agreement exists for other targets. The stripping reactions become more complicated for  $A_T > 1$  because (1) there will be several channels and (2) stripping or pickup to excited states of the target is a contributing factor. We follow the technique used by Serber in reference 33 by assuming there is a surface reaction for nucleon stripping on  ${}^4\text{He}$  and scaling equation (26) by  $A_T^{1/3}$ . Because  ${}^4\text{He}$  is its own mirror nuclei, we ignore the coulomb effects and use equation (26) for both  ${}^3\text{He}$  and  ${}^3\text{H}$  production in the stripping reactions. Note that  ${}^3\text{H}$  is not produced in the stripping reactions with  ${}^1\text{H}$ . A slight overestimate may occur because we expect a small contribution for the  ${}^3\text{He}$  exchange in the reaction  $\alpha + {}^1\text{H} \rightarrow {}^3\text{He} + d$ . We also ignore any  $d$  production in the stripping process for  $A_T > 1$ . Figure 12 shows results for  ${}^3\text{H}$  and  ${}^3\text{He}$  production on  ${}^{12}\text{C}$ . The fragmentation cross section is scaled as  $A_T^{0.31}$  for these fragments. The measurements are from Webber (ref. 27), and the datum at 3.6 GeV/amu is from reference 34.

Table 3 compares the parametric fits with the secondary yields for charge fragments at 3.6 GeV/amu for several targets as measured (ref. 34). The experiment of reference 34 measured only peripheral events with detection angles  $< 5^\circ$ , and we expect the measurements of  ${}^1\text{H}$  secondaries to be underestimates. The multiplicity for nucleon production from  ${}^4\text{He}$  at high energies is between 1 and 1.2 compared with a value of 2 that is assumed in existing cosmic-ray codes. For  ${}^2\text{H}$ , we have used a scaling of  $A_T^{0.4}$  from our parameterization in equation (25).

The multiplicities for proton and neutron production from deuteron projectiles are assumed as unity for transport calculations that ignore pickup reactions. For  ${}^3\text{He}$  and  ${}^3\text{H}$  projectiles, we use a deuteron multiplicity of 0.35 based on calculations (ref. 20), and the nucleon multiplicities are found by balancing the inelastic cross section.

## Secondary Energy Spectrum

The energy spectrum of projectile fragments is determined by the internal momentum distribution of the projectile clusters and a weak dependence on the target caused by dynamical effects. At low energies, kinematical restrictions also limit the energy losses that occur. The energy spectrum of secondaries from light-ion fragmentation is parameterized as

$$\frac{d\sigma}{dE_F} = \sigma_F N_F \exp \left[ - (E - E_0 + C_F)^2 / 2W_F^2 \right] \quad (30)$$

where the width  $W_F$  and the downshift  $C_F$  are in units of MeV/amu and  $E_0$  is the beam kinetic energy in units of MeV/amu. In equation (30), the normalization is given by

$$N_F = \sqrt{\frac{2}{\pi}} \frac{1}{W_F} \frac{1}{\Phi \left[ (E - E_0 + C_F) / \sqrt{2} W_F \right] - \Phi \left[ (-E_0 + C_F) / (\sqrt{2} W_F) \right]} \quad (31)$$

where  $\Phi(x)$  is the error function

$$\Phi(x) = \frac{2}{\sqrt{\pi}} \int_0^x \exp(-u^2) du \quad (32)$$

and  $E_m$  is the maximum kinetic energy of the fragment (if we assume a three-body final state). This kinetic energy is determined by the corresponding maximum momentum:

$$p_M \cong \frac{1}{2\sqrt{S}} \left( \left\{ S - [M_F + (M_P - M_F + \epsilon_B) + M_X]^2 \right\} \left\{ S - [(M_P - M_F + \epsilon_B) + M_X - M_F]^2 \right\} \right)^{1/2} \quad (33)$$

where  $\sqrt{S}$  is the total energy in the three-body center-of-mass frame,  $\epsilon_B$  is the binding energy of the projectile clusters, and  $M$  is the mass. The cumulative spectrum of equation (12) that results from equation (30) is

$$F_{ij}(r, r') = \sigma_F \frac{\left( \Phi \left\{ [\varepsilon(r) - E_0(r') + C_F] / (\sqrt{2}W_F) \right\} - \Phi \left\{ [-E_0(r') + C_F] / (\sqrt{2}W_F) \right\} \right)}{\left( \Phi \left\{ [E_M - E_0(r') + C_F] / (\sqrt{2}W_F) \right\} - \Phi \left\{ [-E_0(r') + C_F] / (\sqrt{2}W_F) \right\} \right)} \quad (34)$$

The energy-dependent parameters  $W_F$  and  $C_F$  are described in reference 20.

The elastically scattered energy spectrum of the alpha particle is parameterized using the Born term of the optical model expansion that is normalized to the coherent model results (ref. 7). A similar approach is followed to parameterize the quasi-elastic energy spectrum. Assuming a Gaussian density matrix for the target, we find from equation (22)

$$\frac{d\sigma}{dE} = 2m_N Z \sigma_{QE} \exp[-2m_N Z (\omega - \epsilon_{B_1})] \theta(\omega - \epsilon_{B_1}) \quad (35)$$

where  $\theta$  is the unit step function and

$$Z = R_T^2 \frac{(R_\alpha^2/2) + B}{(R_\alpha^2/2) + B + R_T^2} \quad (36)$$

The terms  $R_\alpha$  and  $R_T$  denote the matter radii of the alpha particle and target, respectively, and  $B$  is the slope parameter. An energy-dependent parameterization of  $B$  was given in reference 6. Equation (35) is expected to underestimate the spectrum at large  $\omega$  because of multiple scattering and perhaps pion production. The cumulative spectrum that results from equation 35 is

$$F_{ii}(r, r') = \sigma_{QE} \{ \exp[-2m_N Z (E_0 - \epsilon - \epsilon_B)] - \exp[-2m_N Z (E_0 - \epsilon_B)] \} \quad (37)$$

For nucleon-nucleus collisions, the energy spectrum of light target fragments is parameterized (refs. 6 and 7) as

$$\frac{d\sigma_j}{dE} = \frac{\sigma_j}{(2\pi E_{0j}^3)^{1/2}} \sqrt{E} \exp(-E/2E_{0j}) \quad (38)$$

where  $E_{0j}$  is the average energy of target fragment  $j$ . Values for  $E_{0j}$  are derived from the Bertini cascade code (ref. 35) in reference 6. For heavier projectiles, the target fragmentation cross section is scaled as  $A_P^{0.4}$  with the average energy kept at the nucleon value. These assumptions are expected to be only approximately true; however, the dominance of protons and neutrons in the GCR flux may diminish the importance of the accuracy of these assumptions. The most important case for future study will be the target fragment spectra from the incident alpha particles. The cumulative spectrum from equation (38) is

$$F_{ij}(r, r') = \sigma_j \frac{2}{\sqrt{\pi}} \gamma \left( \frac{3}{2}, \frac{E}{2E_{0j}} \right) \quad (39)$$

where  $\gamma(a, x)$  is the incomplete gamma function

$$\gamma(a, x) = \int_0^x \exp(-t) t^{a-1} dt \quad (40)$$

The production spectra of protons and neutrons are estimated using the same mass scaling factor with the evaporation and cascade spectrum described in reference 6.

## Results for Light-Ion Transport

Calculations are now discussed for light-ion production using a solar minimum spectrum from 1977 (ref. 36). Solar modulation occurs over a 22-year cycle with successive solar minimum at approximate 11-year intervals in which maximum particle intensities occur. The 1977 spectrum represents a maximum in this alternating sequence. An estimate of a primary  $^3\text{He}$  component is also made.

Figure 13 shows the energy spectra for  $\alpha$ ,  $h$ ,  $t$ , and  $d$  particles at various shielding depths in a liquid hydrogen shield. These calculations neglect any primary  $d$  or  $h$  component. The  $d$  and  $h$  spectra show two local maxima: the high-energy one at  $\approx 200$  MeV/amu (which corresponds to the peak in the primary  $\alpha$  spectrum,) and the low-energy one below 100 MeV/amu (which is due to the stripping reaction  $\alpha + p \rightarrow ^3\text{He} + d$ ). The fragmentation spectra that are shown are narrow in relation to the energy grid that is normally used in the BRYNTRN code (ref. 7). The narrowness of the spectra leads to an inefficient numerical procedure for particles above several GeV/amu (illustrated in fig. 14) in which the deuteron spectrum at 10 g/cm<sup>2</sup> is plotted for several grid-point values. Integrated quantities such as dose and dose equivalent converge quickly, and only approximately 90 points are needed for an accuracy of a few percent (as shown in table 4 for liquid hydrogen shields) and about 60 points for aluminum shields. Note that the target fragments contribute for the aluminum shields.

Figure 15 gives the calculations for water shields, and figure 16 shows the calculations for aluminum shields. The added source of light ions from target fragmentation is now seen at low energies. For aluminum shields, the target fragments dominate over the projectile fragments  $d, t$ , and  $h$  in the total number of particles and in the expected biological effect, because the target fragments have lower velocities. The distribution between projectile and target effects will be much closer when a primary  $^2\text{H}$  and  $^3\text{He}$  component is included. Approximately 10 percent of the primary He spectrum is the  $^3\text{He}$  isotope with the  $^2\text{H}$  isotopes similar in abundance to  $^3\text{He}$  (ref. 37). Table 5 shows the contributions in dose and dose equivalent with a breakdown in source, either from projectiles or projectile fragments (indicated as PF) or from target fragmentation (indicated as TF), given for aluminum shields.

Figures 17(a) and 17(b) give an estimate of the importance of a primary  $^3\text{He}$  abundance spectrum in transport through liquid hydrogen and aluminum shields. We assume that the  $^3\text{He}$  is 10 percent of the total helium abundance below 100 MeV/amu and that it smoothly rises to 15 percent at high energies (ref. 37). A comparison of figures 13 and 16 with figures 17(a) and 17(b), respectively, shows approximately a factor of 2 increase in  $^3\text{He}$  at moderate shields; this increase is due to the primary component. Table 6 gives a comparison of the dose when  $^3\text{He}$  is considered with and without the primary component for the  $^3\text{He}$  isotopes. Including the primary  $^3\text{He}$  leads to comparable contributions for the projectile-like and the target fragment  $^3\text{He}$  dose equivalent.

Figures 18 and 19 present a breakdown in the neutron flux from primary protons, alpha particles, and a combination of all heavier elements versus the shielding depth for water and aluminum shields. These figures demonstrate that alpha particles produce an important contribution to the total GCR neutron production and that their relative importance increases for lower mass shields. The contribution for neutrons produced from target fragmentation for alpha-induced reactions carries a large uncertainty because of the simple projectile mass scaling to the proton-induced spectra that we have used in our calculations. This uncertainty suggests a need to improve modeling for secondary neutron and proton and deuteron production for alpha-induced target fragmentation. Comparisons with experimental data (refs. 38 and 39) for monoenergetic alpha-particle beams could also be made.

## Concluding Remarks

The space radiation transport code BRYNTRN was modified to transport cosmic-ray helium nuclei and their secondaries. A data base for light-ion fragmentation was discussed and implemented

into the transport code. Light ions produced in target fragmentation events were also transported, which will allow their effects on linear or lineal energy spectra to be evaluated and considered for further nuclear collisions by the helium particles. The contribution of neutron production by galactic cosmic ray (GCR) alpha particles was estimated to be significant, thus indicating that improvements in target fragmentation cross sections for light ions should be made in the future. The finite widths of the secondary spectrum from light-ion fragmentation were shown to lead to a slow convergence in the transport algorithms above approximately 5 GeV/amu, thus suggesting that numerical methods should be developed for improving this convergence. Measurements of the nucleon component in these events and estimates of stripping and pickup cross sections above and below pion-production thresholds are the most important information for validating the light-ion data base. The extension of the cosmic-ray space radiation transport code for isotope transport allows a more detailed study of the isotopic composition of the primary GCR.

NASA Langley Research Center  
Hampton, VA 23681-0001  
July 13, 1993

## References

1. Webber, W. R.: *Handbuch der Physik, Band XLVI/2*. Springer-Verlag, 1967.
2. Cucinotta, Francis A.; Townsend, Lawrence W.; Wilson, John W.; Golightly, Michael J.; and Weyland, Mark: Analysis of Radiation Risk From Alpha Component of Solar Particle Events. *Advances in Space Research*, 1994.
3. Fichtel, C. E.: Solar Cosmic Rays. *Philos. Trans. Royal Soc. London*, ser. A, vol. 270, no. 1202, July 16, 1971, pp. 167-174.
4. Wilson, John W.; and Lamkin, Stanley L.: Perturbation Theory for Charged-Particle Transport in One Dimension. *Nucl. Sci. & Eng.*, vol. 57, no. 4, Aug. 1975, pp. 292-299.
5. Wilson, John W.: *Heavy Ion Transport in the Straight Ahead Approximation*. NASA TP-2178, 1983.
6. Wilson, John W.; Townsend, Lawrence W.; Nealy, John E.; Chun, Sang Y.; Hong, B. S.; Buck, Warren W.; Lamkin, S. L.; Ganapol, Barry D.; Khan, Ferdous; and Cucinotta, Francis A.: *BRYNTRN: A Baryon Transport Model*. NASA TP-2887, 1989.
7. Wilson, John W.; Townsend, Lawrence W.; Schimmerling, Walter; Khandelwal, Govind S.; Khan, Ferdous; Nealy, John E.; Cucinotta, Francis A.; Simonsen, Lisa C.; Shinn, Judy L.; and Norbury, John W.: *Transport Methods and Interactions for Space Radiations*. NASA RP-1257, 1991.
8. Townsend, Lawrence W.; Cucinotta, Francis A.; Shinn, Judy L.; and Wilson, John W.: *Effects of Fragmentation Parameter Variations on Estimates of Galactic Cosmic Ray Exposure—Dose Sensitivity Studies for Aluminum Shields*. NASA TM-4386, 1992.
9. Shinn, Judy L.; Wilson, John W.; Weyland, Mark; and Cucinotta, Francis A.: *Improvements in the Computational Accuracy of BRYNTRN (A Baryon Transport Code)*. NASA TP-3093, 1991.
10. Andersen, H. H.; and Ziegler, J. F.: *Hydrogen—Stopping Powers and Ranges in All Elements*. Volume 3 of *The Stopping and Ranges of Ions in Matter*, J. F. Ziegler, organizer, Pergamon Press Inc., c.1977.
11. Ziegler, J. F.: The Electronic and Nuclear Stopping of Energetic Ions. *Appl. Phys. Lett.*, vol. 31, no. 8, Oct. 15, 1977, pp. 544-546.
12. Ziegler, J. F.: *Helium—Stopping Powers and Ranges in All Elemental Matter*. Volume 4 of *The Stopping and Ranges of Ions in Matter*, J. F. Ziegler, organizer, Pergamon Press Inc., c.1977.
13. Lindhard, J.; Scharff, M.; and Schiott, H. E.: Range Concepts and Heavy Ion Ranges (Notes on Atomic Collisions, II). *Mat.-Fys. Medd.—K. Dan. Vidensk. Selsk.*, vol. 33, no. 14, 1963, pp. 1-42.
14. Cucinotta, Francis A.; Townsend, Lawrence W.; Wilson, John W.; and Khandelwal, Govind S.: *Inclusive Inelastic Scattering of Heavy Ions and Nuclear Correlations*. NASA TP-3026, 1990.
15. Cucinotta, Francis A.; Townsend, Lawrence W.; and Wilson, John W.: Inclusive Inelastic Scattering of Heavy Ions in the Independent Particle Model. *J. Physics G: Nucl. Particle Phys.*, vol. 18, no. 5, May 1992, pp. 889-901.

16. Cucinotta, Francis A.; Townsend, Lawrence W.; Wilson, John W.; and Norbury, John W.: *Corrections to the Participant-Spectator Model of High-Energy Alpha Particle Fragmentation*. NASA TM-4262, 1991.
17. Cucinotta, Francis A.; Townsend, Lawrence W.; and Wilson, John W.: Production of  $^3\text{H}$  at Large Momentum in  $\alpha$ - $^{12}\text{C}$  Collisions at 2A GeV. *Phys. Lett. B*, vol. 282, no. 1, 2, May 21, 1992, pp. 1–6.
18. Cucinotta, Francis A.; Townsend, Lawrence W.; and Wilson, John W.: *Quasi-Elastic Nuclear Scattering at High Energies*. NASA TM-4362, 1992.
19. Cucinotta, Francis A.; Townsend, Lawrence W.; and Wilson, John W.: Multiple-Scattering Effects in Quasielastic  $\alpha$ - $^4\text{He}$  Scattering. *Phys. Review C*, vol. 46, no. 4, Oct. 1992, pp. 1451–1456.
20. Cucinotta, Francis A.; Townsend, Lawrence W.; and Wilson, John W.: *Description of Alpha-Nucleus Interaction Cross Sections for Cosmic Ray Shielding Studies*. NASA TP-3285, 1993.
21. Ableev, V. G.; Bodyagin, V. A.; Vorob'ev, G. G.; Zaporozhets, S. A.; Nomofilov, A. A.; Piskunov, N. M.; Sitnik, I. M.; Stokovskii, E. A.; Strunov, L. N.; Tarasov, A. V.; Filipkovski, A.; Khristova, I. U.; and Sharov, V. I.: Scattering of 17.9 GeV/c  $\alpha$  Particles by C, Al, and Cu Nuclei. *Sov. J. Nucl. Phys.*, vol. 36, no. 5, Nov. 1982, pp. 698–703.
22. Bizard, G.; Le Brun, C.; Berger, J.; Duflo, J.; Goldzahl, L.; Plouin, F.; Oostens, J.; Van den Bossche, M.; Vu Hai, L.; Fabbri, F. L.; Picozza, P.; and Satta, L.:  $^3\text{He}$  Production in  $^4\text{He}$  Fragmentation on Protons at 6.85 GeV/c. *Nucl. Phys.*, vol. A285, no. 3, Aug. 1, 1977, pp. 461–468.
23. Ableev, V. G.; Dshemuchadse, S. V.; Dimitrov, C.; Kobushkin, A. P.; Naumann, B.; Naumann, L.; Nomofilov, A. A.; Penchev, L.; Piskunov, N. M.; Sharov, V. I.; Sitnik, I. M.; Stokovsky, E. A.; Strunov, L. N.; Tesch, S.; and Zaporozhets, S. A.: Proton and Triton Momentum Distributions for  $^4\text{He}$  Fragmentation at Relativistic Energies. *Few-Body Syst.*, vol. 8, 1990, pp. 137–144.
24. Anderson, L.; Brückner, W.; Moeller, E.; Nagamiya, S.; Nissen-Meyer, S.; Schroeder, L.; Shapiro, G.; and Steiner, H.: Inclusive Particle Production at Forward Angles From Collisions of Relativistic Nuclei: Nuclear Fragments. *Phys. Review C*, third ser., vol. 28, no. 3, Sept. 1983, pp. 1224–1245.
25. Anderson, L.; Moeller, E.; Nagamiya, S.; Nissen-Meyer, S.; Schroeder, L.; Shapiro, G.; and Steiner, H.: *Inclusive Particle Production at Forward Angles From Collisions of Light Relativistic Nuclei, Part III: Data Tables*. LBL-14330 (Contract DE-AC03-76SF00098), Dep. of Physics, Univ. of California, May 1982.
26. Meyer, J. P.: Deuterons and  $\text{He}^3$  Formation and Destruction in Proton Induced Spallation of Light Nuclei/Z Less Than or Equal to 8/. *Astron. & Astrophys. Suppl.*, vol. 7, no. 4, Dec. 1972, pp. 417–467.
27. Webber, W. R.: New Measurements of the Cross Sections of  $^4\text{He}$  Into  $^2\text{H}$  and  $^3\text{He}$  and Their Implication for  $^2\text{H}$  and  $^3\text{He}$  Production in Cosmic Rays. *Particle Astrophysics—The NASA Cosmic Ray Program for the 1990s and Beyond*, W. V. Jones, Frank J. Kerr, and Jonathan F. Ormes, eds., American Inst. of Physics, 1990, pp. 294–298.
28. Bildsten, Lars; Wasserman, Ira; and Salpeter, Edwin E.: A Semi-Classical Model for Breakup Reactions of Light Nuclei:  $^4\text{He}(p, pn) ^3\text{He}$ . *Nucl. Phys.*, vol. A516, no. 1, Sept. 17, 1990, pp. 77–107.
29. Sourkes, A. M.; Houdayer, A.; Van Oers, W. T. H.; Carlson, R. F.; and Brown, Ronald E.: Total Reaction Cross Section for Protons on  $^3\text{He}$  and  $^4\text{He}$  Between 18 and 48 MeV. *Phys. Review C*, third ser., vol. 13, no. 2, Feb. 1976, pp. 451–460.
30. Aladashvili, B. S.; Bánó, M.; Braun, H.; Gerber, J. P.; Glagolev, V. V.; Gorbunov, A. N.; Hlaváčová, J.; Juillot, P.; Khairtdinov, K. U.; Lebedev, R. M.; Martinská, G.; Menteshashvili, Z. R.; Michalon, A.; Mirianashvili, D. G.; Nioradze, M. S.; Patočka, J.; Seman, M.; Sobszak, T.; Stepaniak, J.; Streltsov, V. N.; Šándor, L.; Urban, J.; Zhuravleva, L. I.; and Futó, A.: Production of Deuterons in a  $^4\text{He}$ -p Interaction at 8.6 GeV/c. *Acta Phys. Slov.*, vol. 31, no. 1, 1981, pp. 29–37.
31. Fiarman, S.; and Meyerhof, W. E.: Energy Levels of Light Nuclei  $A = 4$ . *Nucl. Phys.*, vol. A206, no. 1, May 14, 1973, pp. 1–64.
32. Townsend, L. W.; and Wilson, J. W.: Energy-Dependent Parameterization of Heavy Ion Absorption Cross Sections. *Radiat. Res.*, vol. 106, 1986, pp. 283–287.
33. Serber, R.: The Production of High Energy Neutrons by Stripping. *Phys. Review*, second ser., vol. 72, no. 11, July 1–Dec. 15, 1947, pp. 1008–1016.
34. Abdurakhimov, A. Kh.; Anikina, M. Kh.; Buttsev, V. S.; et al.: A Study of Pion Production in 4.5 (GeV/c) Nucleon  $^4\text{He}$  Interactions With Nuclear Targets. *Nucl. Phys.*, vol. A362, no. 2, June 8, 1981, pp. 376–390.

35. Bertini, Hugo W.; Guthrie, Miriam P.; and Culkowski, Arline H.: *Nonelastic Interactions of Nucleons and  $\pi$ -Mesons With Complex Nuclei at Energies Below 3 GeV*. ORNL-TM-3148, U.S. Atomic Energy Commission, Mar. 28, 1972.
36. Badhwar, Gautam D.; Cucinotta, Francis A.; and O'Neill, Patrick M.: Depth-Dose Equivalent Relationship for Cosmic Rays at Various Solar Minima. *Radiat. Res.*, vol. 134, 1993, pp. 9–15.
37. Webber, W. R.; and Yushak, S. M.: A Measurement of the Energy Spectra and Relative Abundance of the Cosmic-Ray H and He Isotopes Over a Broad Energy Range. *Astrophys. J.*, vol. 275, no. 1, pt. 1, Dec. 1, 1983, pp. 391–404.
38. Smith, A. R.; Schimmerling, W.; Henson, A. M.; Kanstein, L. L.; McCaslin, J. B.; Stephens, L. D.; Thomas, R. H.; Ozawa, J.; and Yeater, F. W.: *Neutron Flux Density and Secondary-Particle Energy Spectra at the 184-Inch Synchrocyclotron Medical Facility*. LBL-6721 (Contract No. W-7405-ENG-48), Univ. of California, July 1978.
39. Parizet, M. J.; Alard, J. P.; Rahmani, A.; Montarou, G.; Augerat, J.; Bastid, N.; Demaison, P.; Dupieux, P.; Fraysse, L.; Marroncle, J.; Raha, S.; Babinet, R.; Fodor, Z.; Gosset, J.; L'Hote, D.; Poitou, J.; Schimmerling, W.; Terrien, Y.; Valette, O.; Lemaire, M. C.; Gorodetzky, P.; and Racca, C.: Proton Production in Relativistic Heavy Ion Collisions; Comparison With a Thermodynamical Model. *Int. J. Modern Phys. A*, vol. 4, no. 14, 1989, pp. 3689–3703.

Table 1. Comparisons of Calculations With Experiments for  
 $A = 3$  Fragment Production From  ${}^4\text{He}$

[Calculations in parentheses; experimental data from Webber (ref. 27)]

(a)  $\alpha + {}^{12}\text{C} \rightarrow A_F$

$T_{\text{lab}}$ , MeV/amu	$\sigma_{3\text{H}}$ , mb	$\sigma_{3\text{He}}$ , mb
203.3	$93.1 \pm 9.3$ (77.2)	$60.4 \pm 6$ (79.3)
377.1	$79 \pm 7.9$ (59.9)	$66.9 \pm 6.7$ (60.9)
519.9	– (62.1)	$69.4 \pm 6.9$ (59.8)

(b)  $\alpha + {}^1\text{H} \rightarrow A_F$

$T_{\text{lab}}$ , MeV/amu	$\sigma_{3\text{He}}$ , mb
377.1	$26.3 \pm 2.6$ (19.5)
519.9	$26.4 \pm 2.6$ (20.8)
1025.0	$24.1 \pm 1.9$ (22.5)

Table 2. Thresholds and  $Q$ -Values for  $p + {}^4\text{He}$

Reaction	$Q$ , MeV (a)	Threshold, MeV
${}^4\text{He}(p, d){}^3\text{He}$	–18.354	22.94
${}^4\text{He}(p, 2p){}^3\text{He}$	–19.815	24.77
${}^4\text{He}(p, pn){}^3\text{He}$	–20.578	25.72
${}^4\text{He}(p, pd){}^2\text{H}$	–23.848	29.81
${}^4\text{He}(p, pd){}^2\text{H}$	–26.072	32.59
${}^4\text{He}(p, ppnn){}^1\text{H}$	–28.297	35.37

<sup>a</sup>Data taken from reference 31.

Table 3. Comparison of Experimental Fragmentation Cross Sections for  
 ${}^4\text{He}$  Projectiles at 3.6 GeV/amu With Model Fits

[Model fits in parentheses]

Fragment	Values of $\sigma_F$ , mb, for target $s^a$ of –			
	Li	C	Al	Cu
${}^1\text{H}$	$166 \pm 13$ (536.6)	$227 \pm 20$ (592.0)	$319 \pm 34$ (823.9)	$417 \pm 45$ (1294.9)
${}^2\text{H}$	$84 \pm 15$ (68.2)	$91 \pm 27$ (91.2)	$113 \pm 38$ (128.2)	$159 \pm 45$ (184.2)
${}^3\text{H}$	$47 \pm 5$ (52.7)	$58 \pm 9$ (65.4)	$73 \pm 20$ (84.1)	$95 \pm 14$ (109.9)
${}^3\text{He}$	$48 \pm 5$ (48.1)	$49 \pm 8$ (59.6)	$70 \pm 15$ (76.7)	$95 \pm 20$ (100.2)

<sup>a</sup>Data taken from experiments in reference 27 which measured only particles in peripheral events ( $\theta \leq 5^\circ$ ).

Table 4. Convergence of Light-Ion Dose and Dose Equivalent

[Dose equivalent in parentheses]

(a) Liquid hydrogen shields

Particles	$N = 60$		$N = 90$		$N = 120$	
	$D, \text{cGy} (H, \text{cSv})$		$D, \text{cGy} (H, \text{cSv})$		$D, \text{cGy} (H, \text{cSv})$	
$3 \text{ g/cm}^2$						
$d$	0.057	(0.060)	0.063	(0.066)	0.065	(0.068)
$t$	.071	(.073)	.081	(.083)	.087	(.089)
$h$	.093	(.128)	.103	(.138)	.107	(.141)
$\alpha$	2.560	(2.955)	2.560	(2.954)	2.560	(2.954)
$10 \text{ g/cm}^2$						
$d$	0.126	(0.130)	0.142	(0.146)	0.149	(0.153)
$t$	.143	(.143)	.159	(.163)	.171	(.174)
$h$	.192	(.192)	.172	(.211)	.183	(.219)
$\alpha$	1.278	(1.461)	1.278	(1.460)	1.278	(1.460)
$40 \text{ g/cm}^2$						
$d$	0.118	(0.121)	0.135	(0.138)	0.144	(0.147)
$t$	.070	(.072)	.080	(.082)	.086	(.087)
$h$	.050	(.061)	.062	(.073)	.064	(.079)
$\alpha$	.071	(.082)	.071	(.081)	.071	(.081)

(b) Aluminum shields

Particles	$N = 45$		$N = 60$		$N = 90$	
	$D, \text{cGy} (H, \text{cSv})$		$D, \text{cGy} (H, \text{cSv})$		$D, \text{cGy} (H, \text{cSv})$	
$3 \text{ g/cm}^2$						
$d$	0.355	(1.352)	0.350	(1.351)	0.353	(1.357)
$t$	.092	(.466)	.093	(.468)	.095	(.471)
$h$	.044	(.480)	.045	(.483)	.046	(.484)
$\alpha$	3.571	(8.759)	3.575	(8.743)	3.575	(8.758)
$10 \text{ g/cm}^2$						
$d$	0.386	(1.473)	0.387	(1.482)	0.395	(1.500)
$t$	.117	(.535)	.122	(.546)	.126	(.551)
$h$	.065	(.546)	.069	(.554)	.074	(.599)
$\alpha$	3.168	(8.693)	3.176	(8.708)	3.179	(8.740)
$40 \text{ g/cm}^2$						
$d$	0.435	(1.638)	0.461	(1.712)	0.486	(1.763)
$t$	.155	(.646)	.169	(.679)	.183	(.701)
$h$	.092	(.624)	.104	(.654)	.119	(.677)
$\alpha$	1.929	(7.788)	1.957	(7.987)	1.968	(8.116)

Table 5. Dose and Dose Equivalent From Light Ions in Aluminum Shields

[Dose equivalent in parentheses]

Particles	PF <sup>a</sup>		TF <sup>b</sup>		Total	
	<i>D</i> , cGy ( <i>H</i> , cSv)		<i>D</i> , cGy ( <i>H</i> , cSv)		<i>D</i> , cGy ( <i>H</i> , cSv)	
3 g/cm <sup>2</sup>						
<i>d</i>	0.011	(0.012)	0.342	(1.345)	0.353	(1.357)
<i>t</i>	.013	(.015)	.082	(.446)	.095	(.471)
<i>h</i>	.016	(.026)	.030	(.458)	.046	(.484)
$\alpha$	3.310	(4.055)	0.265	(4.703)	3.575	(8.758)
10 g/cm <sup>2</sup>						
<i>d</i>	0.034	(0.035)	0.361	(1.465)	0.395	(1.500)
<i>t</i>	.038	(0.043)	.092	(.508)	.126	(0.551)
<i>h</i>	.041	(0.060)	.033	(.499)	.074	(0.559)
$\alpha$	2.890	(3.533)	0.289	(5.207)	3.179	(8.740)
40 g/cm <sup>2</sup>						
<i>d</i>	0.144	(0.147)	0.342	(1.616)	0.486	(1.763)
<i>t</i>	.086	(.087)	.097	(.614)	.183	(.701)
<i>h</i>	.068	(.079)	.051	(.598)	.119	(.677)
$\alpha$	.071	(.081)	1.897	(8.035)	1.968	(8.116)

<sup>a</sup>PF represents contributions from projectile fragments.

<sup>b</sup>TF represents contributions caused by target fragments.

Table 6. Dose and Dose-Equivalent Contributions From <sup>3</sup>He in Shielding Materials

[Dose equivalent in parentheses]

(a) Liquid hydrogen shields

<i>x</i> , g/cm <sup>2</sup>	With primary <sup>3</sup> He		Without primary <sup>3</sup> He	
	<i>D</i> , cGy ( <i>H</i> , cSv)		<i>D</i> , cGy ( <i>H</i> , cSv)	
3	0.500	(0.577)	0.107	(0.141)
5	.485	(.583)	.144	(.182)
10	.424	(.485)	.183	(.219)
20	.286	(.325)	.162	(.189)
40	.103	(.117)	.068	(.079)

(b) Aluminum shields

<i>x</i> , g/cm <sup>2</sup>	With primary <sup>3</sup> He		Without primary <sup>3</sup> He	
	<i>D</i> , cGy ( <i>H</i> , cSv)		<i>D</i> , cGy ( <i>H</i> , cSv)	
3	0.515	(1.026)	0.046	(0.484)
5	.511	(1.038)	.057	(.523)
10	.495	(1.051)	.074	(.559)
20	.459	(1.045)	.095	(.662)
40	.390	(1.00)	.119	(.677)

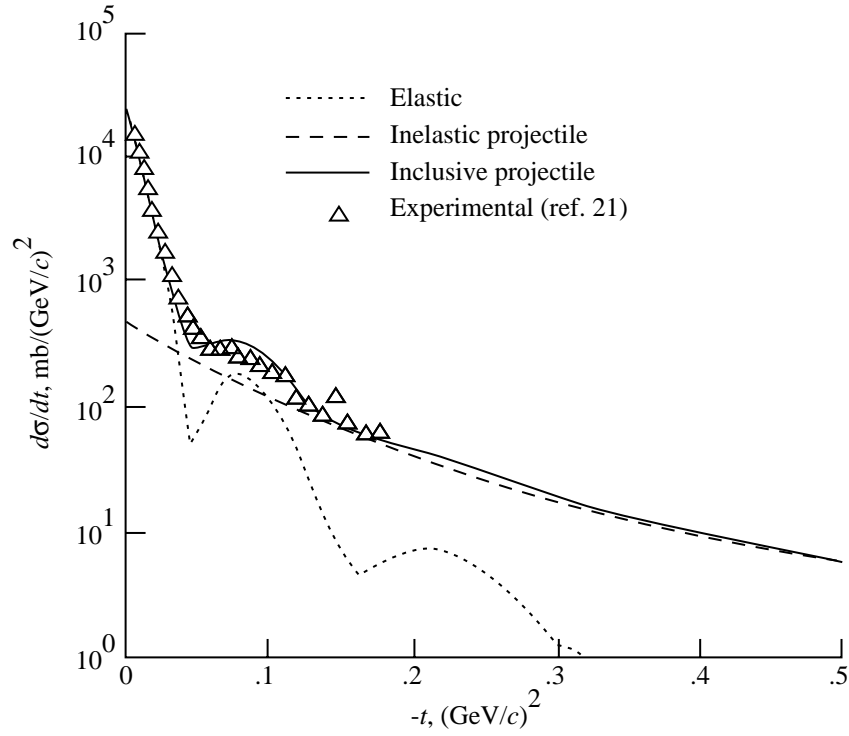


Figure 1. Inclusive  ${}^4\text{He} + {}^{12}\text{C}$  scattering distributions at 3.6 GeV/amu versus invariant momentum transfer.

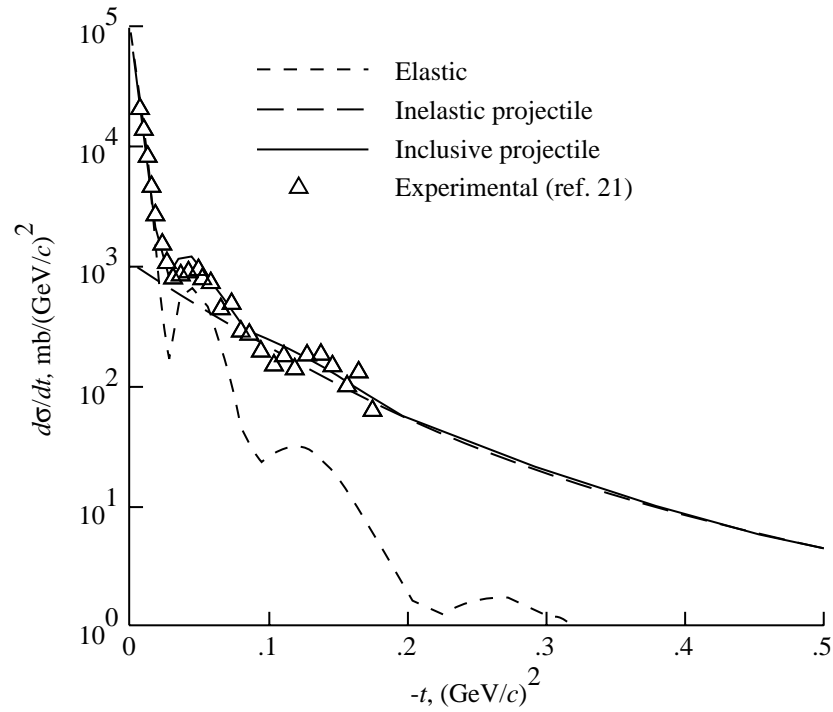


Figure 2. Inclusive  ${}^4\text{He} + {}^{27}\text{Al}$  scattering distributions at 3.6 GeV/amu versus invariant momentum transfer.

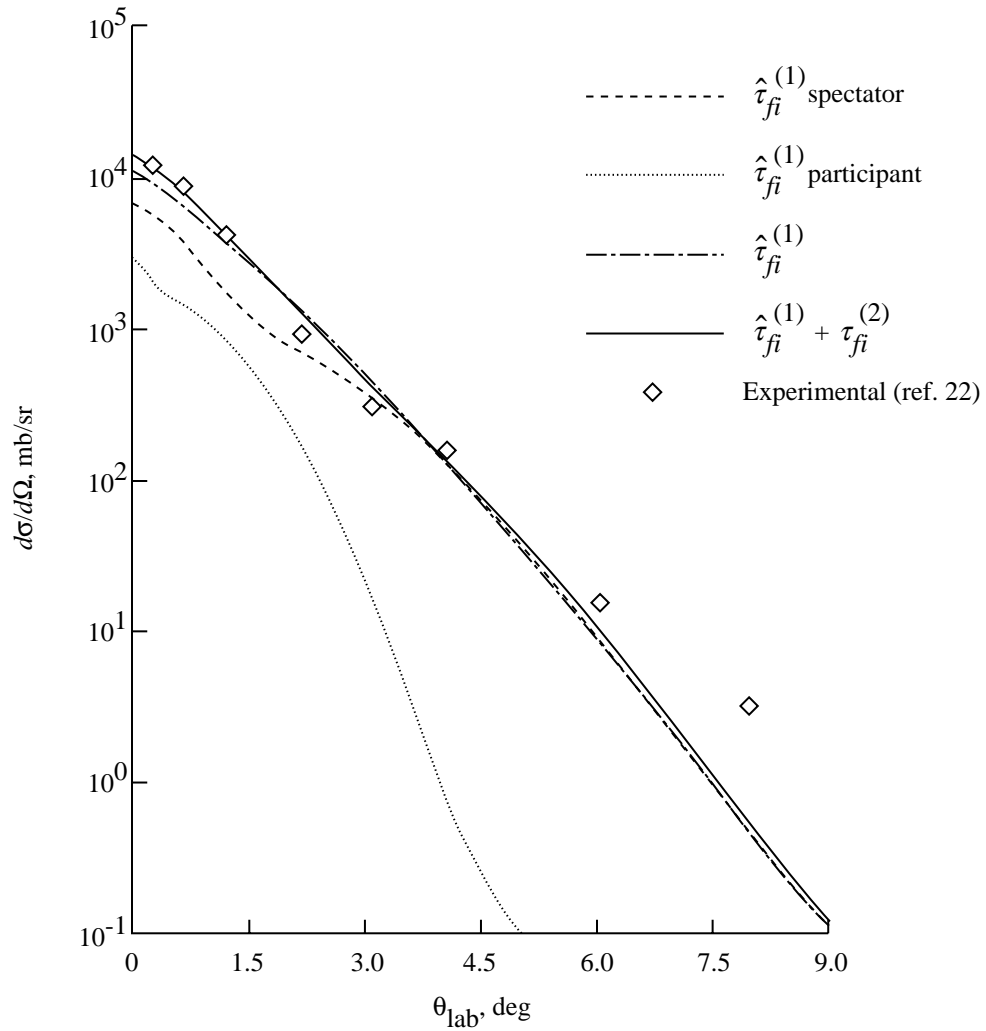


Figure 3. Angular distribution for  $\alpha + {}^1\text{H} \rightarrow {}^3\text{He}$  at 1.02 GeV/amu.

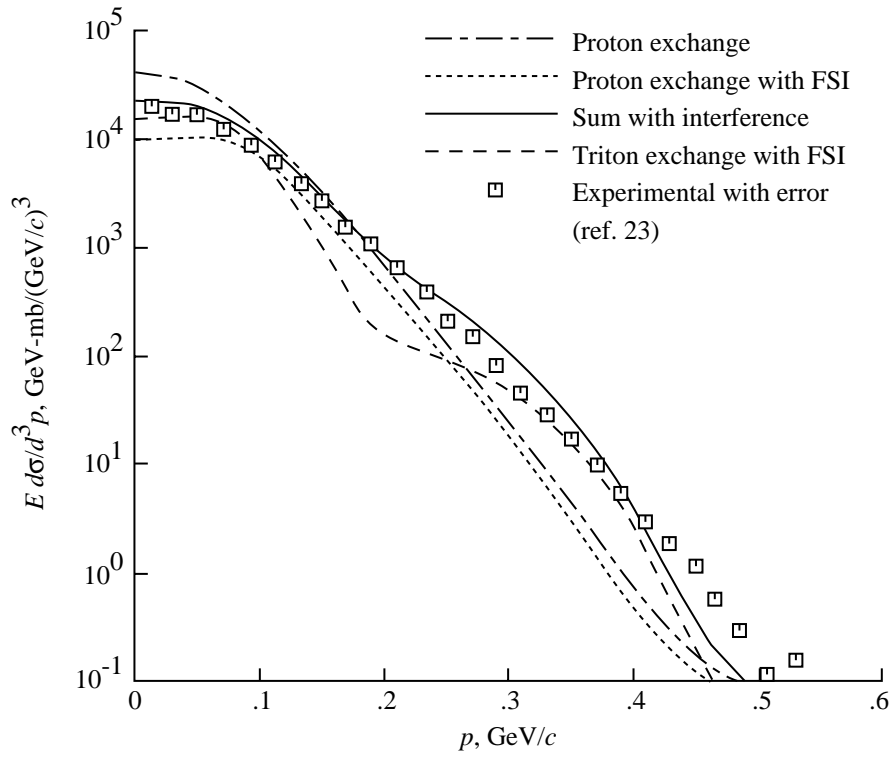


Figure 4. Comparison of calculations of longitudinal momentum distribution for  ${}^3\text{H}$  production in  ${}^4\text{He} + {}^{12}\text{C}$  collisions at 1.9 GeV/amu with experiment (ref. 23).

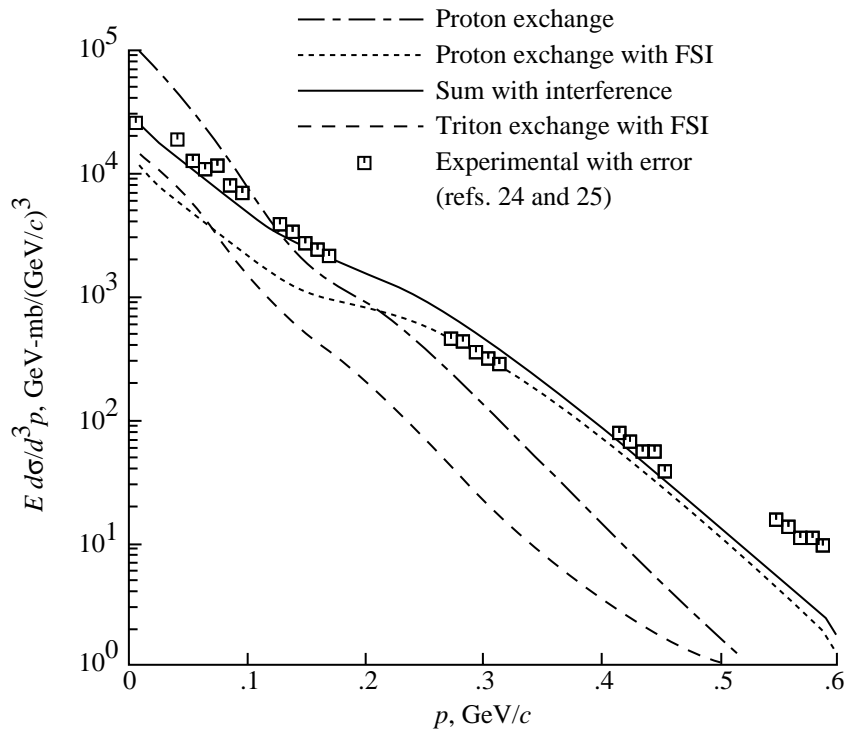


Figure 5. Comparison of calculations of transverse momentum distribution for  ${}^3\text{H}$  production in  ${}^4\text{He} + {}^{12}\text{C}$  collisions at 0.385 GeV/amu with experimental data.

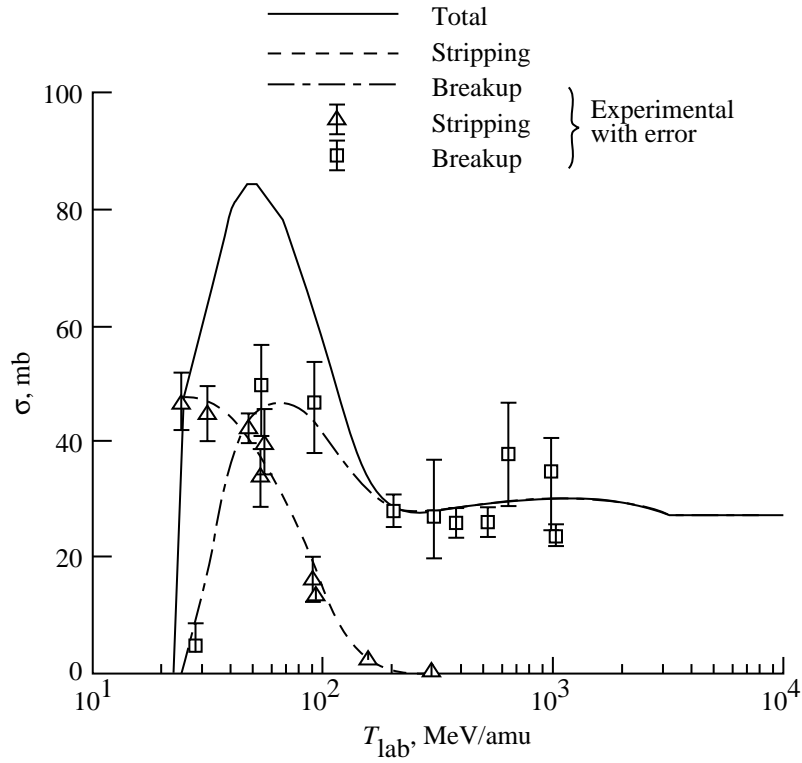


Figure 6. Comparison of parametric model for  ${}^3\text{He}$  production in  $\alpha + {}^1\text{H}$  collisions with experimental data.

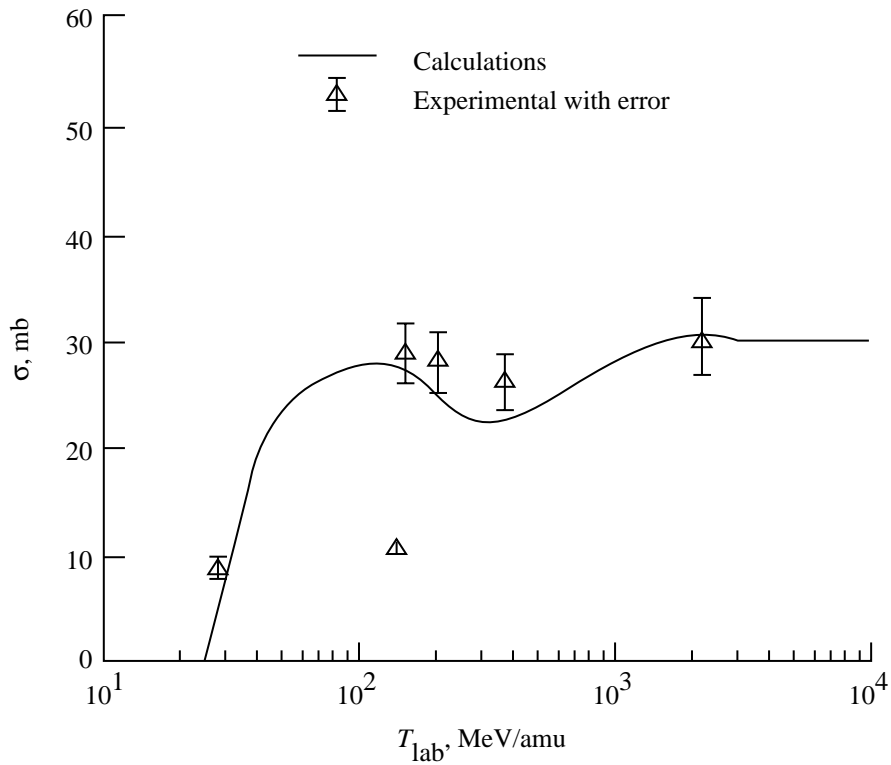


Figure 7. Comparison of parametric model for  ${}^3\text{H}$  production in  $\alpha + {}^1\text{H}$  collisions with experimental data.

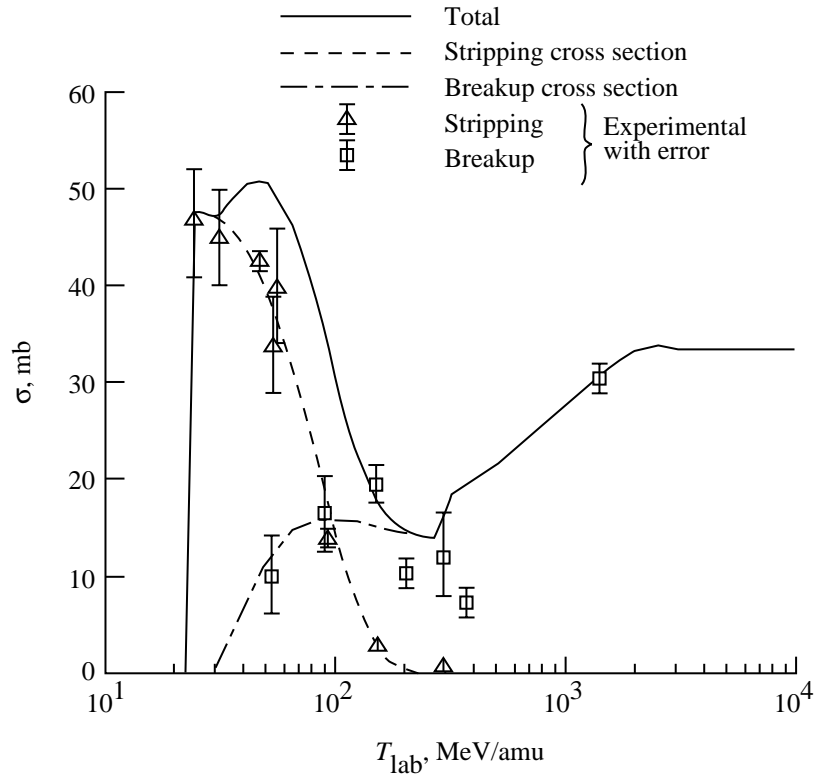


Figure 8. Comparison of parametric model  $^2\text{H}$  production in  $\alpha + ^1\text{H}$  collisions with experimental data.

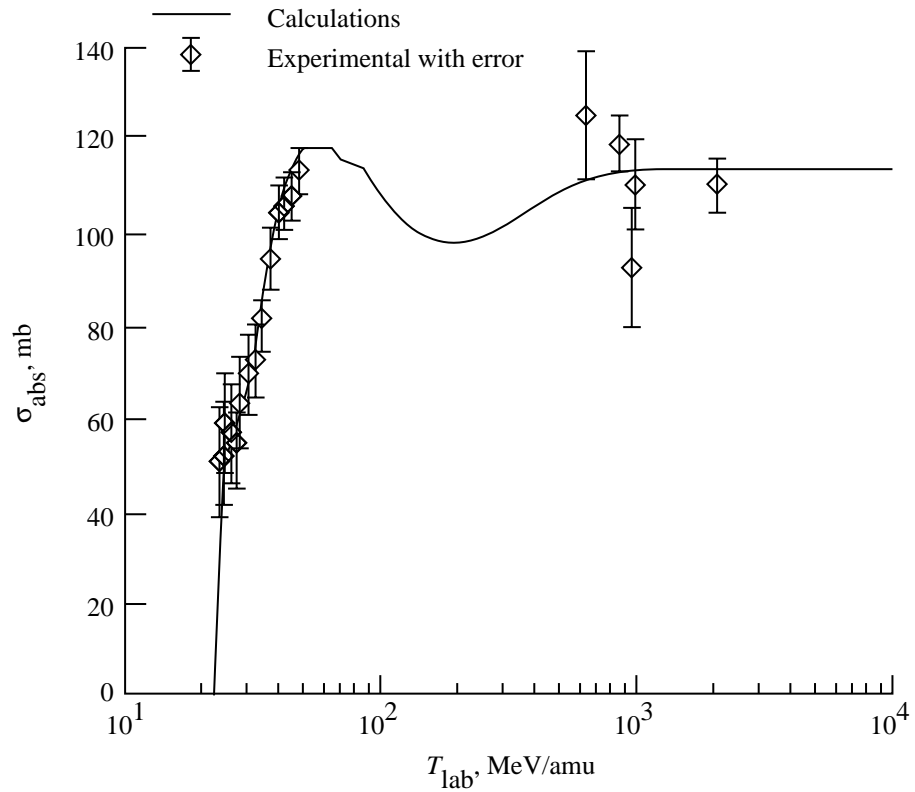


Figure 9. Comparison of parametric model for  $\alpha + ^1\text{H}$  absorption cross section with experimental data.

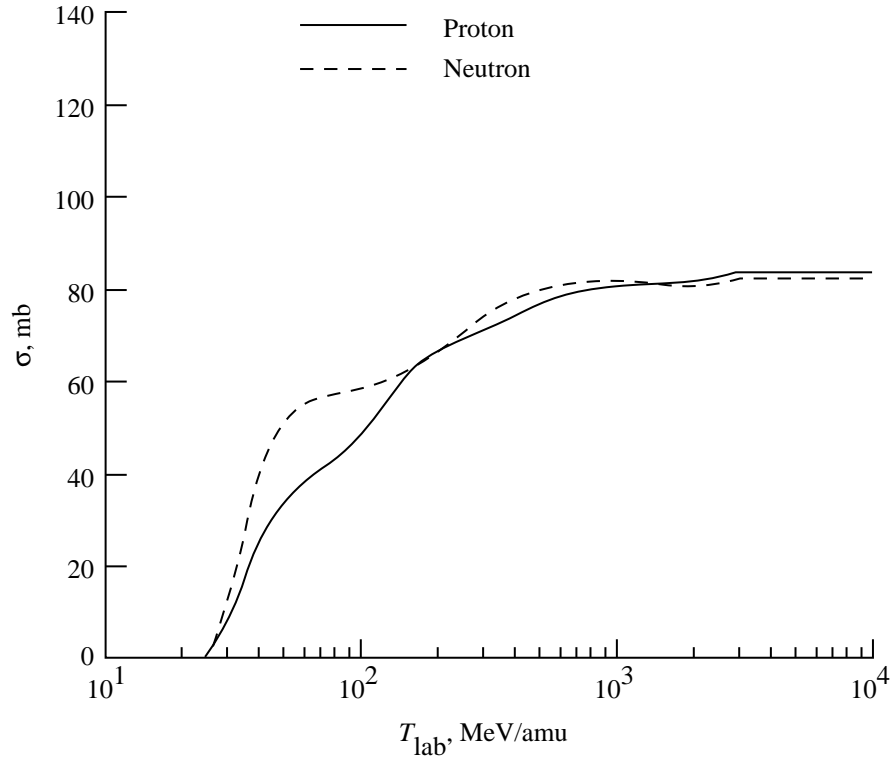


Figure 10. Parametric model predictions for proton production and neutron production in  $\alpha + {}^1\text{H}$  collisions.

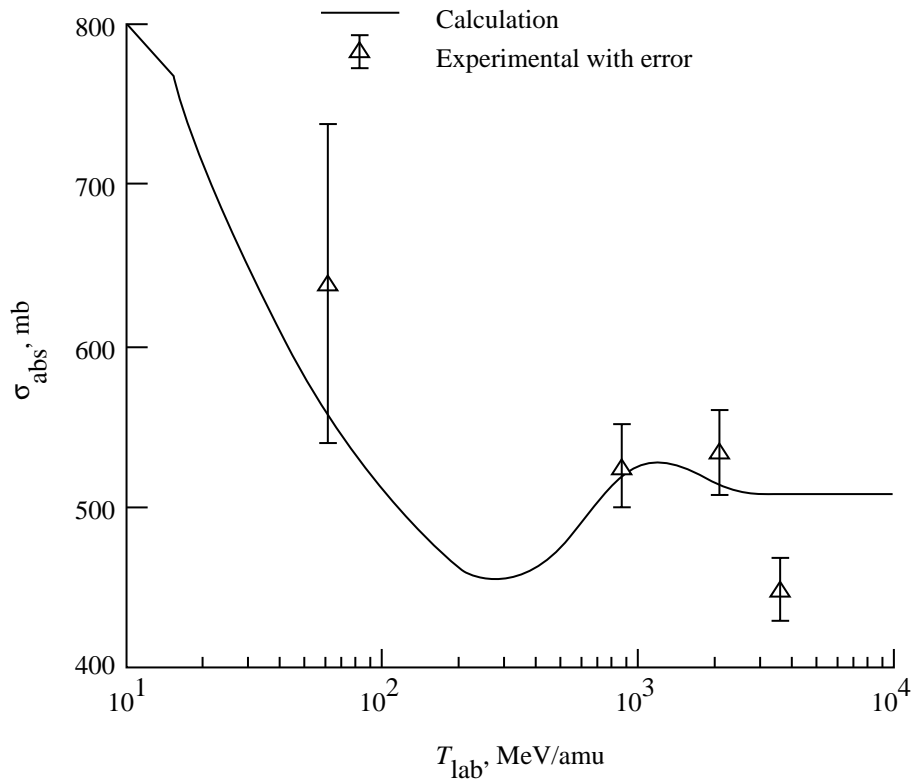


Figure 11. Comparison of parametric model for  ${}^4\text{He} + {}^{12}\text{C}$  absorption cross sections with experimental data.

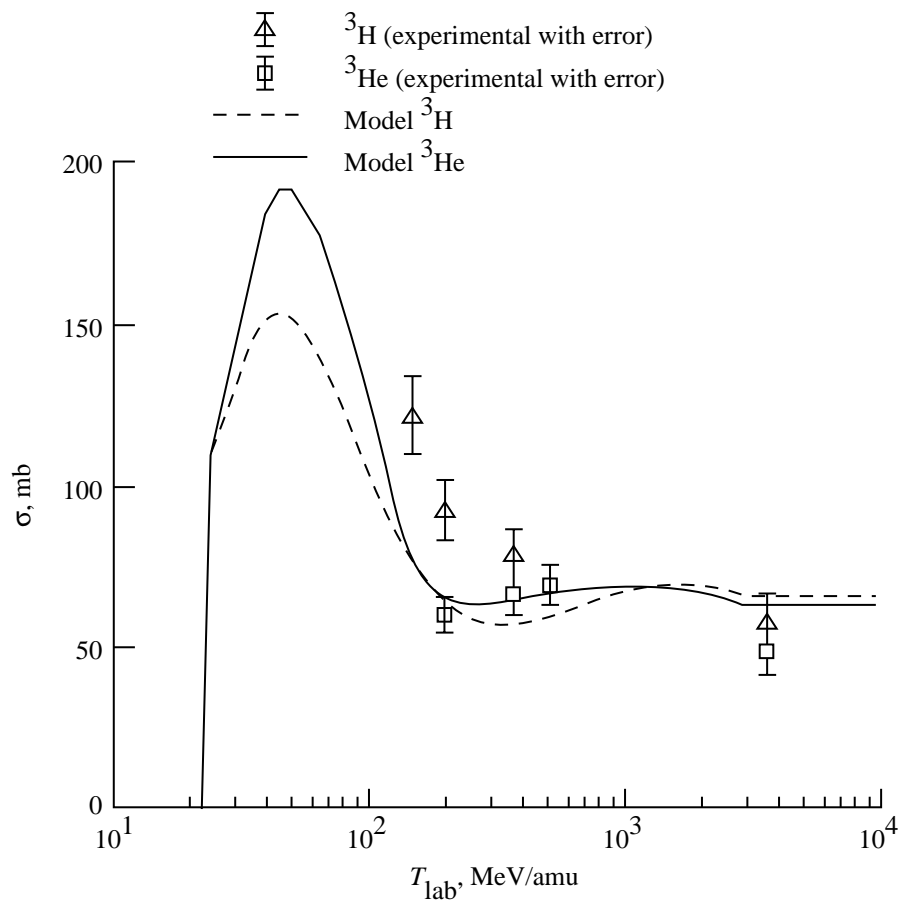


Figure 12. Comparison of fits for  ${}^3\text{He}$  and  ${}^3\text{H}$  production cross sections in  ${}^4\text{He} + {}^{12}\text{C}$  collisions with experimental data.

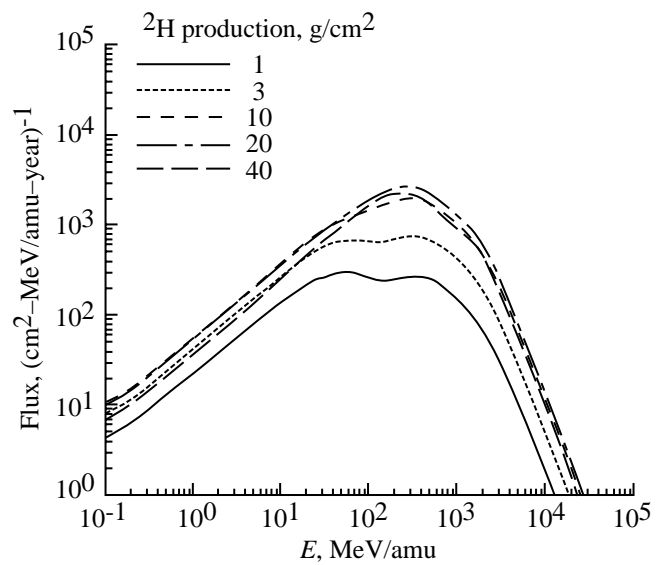
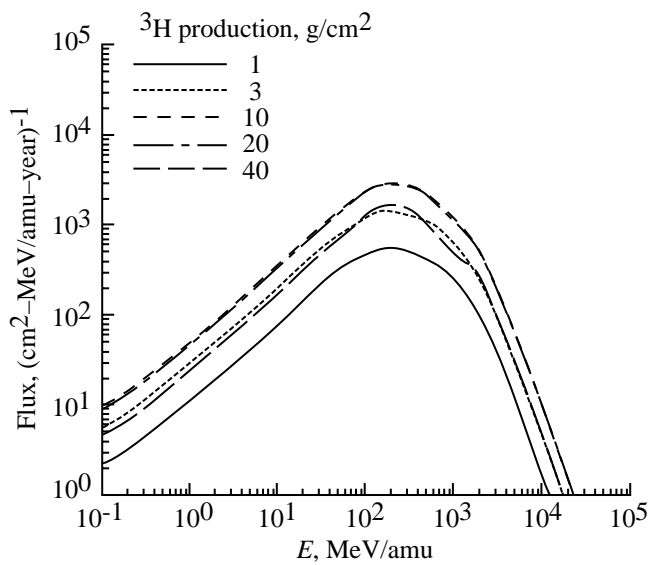
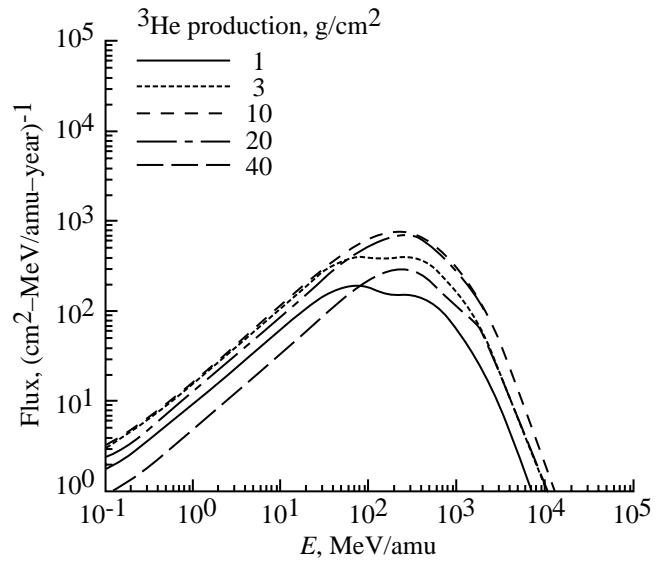
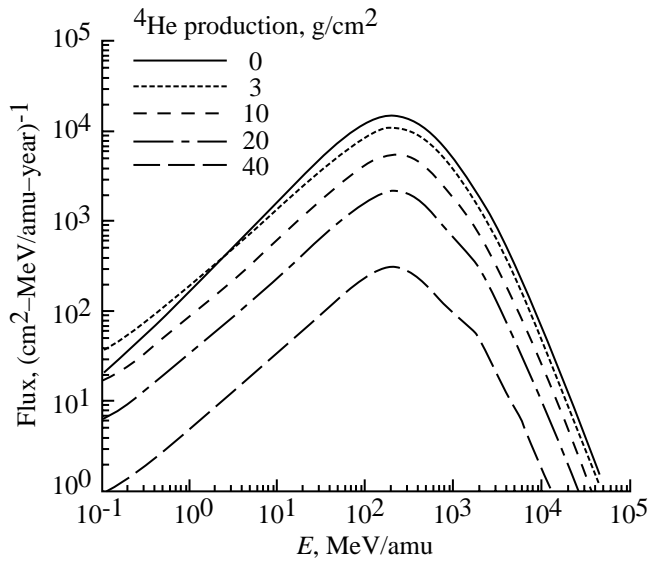


Figure 13. Calculations of light-ion flux spectrum in liquid hydrogen.

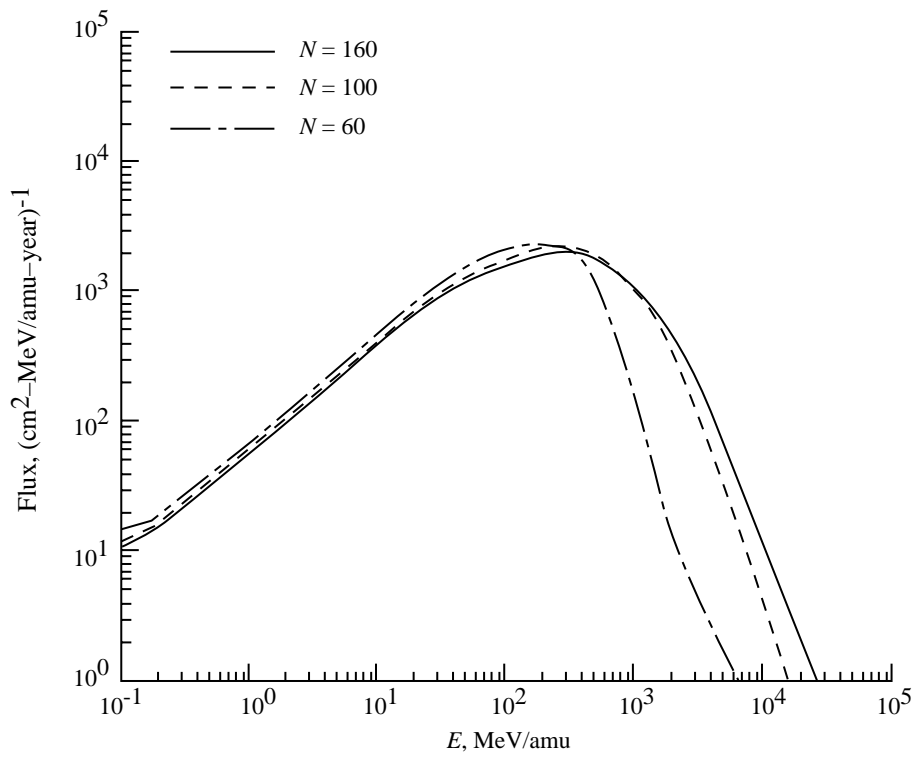


Figure 14. Comparison of deuteron flux spectra in  $10 \text{ g/cm}^2$  of  $\text{H}_2$  shields for several grid values.

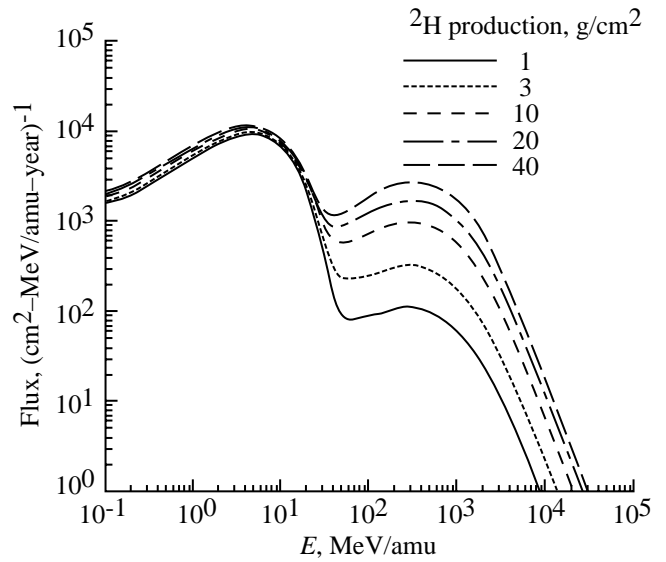
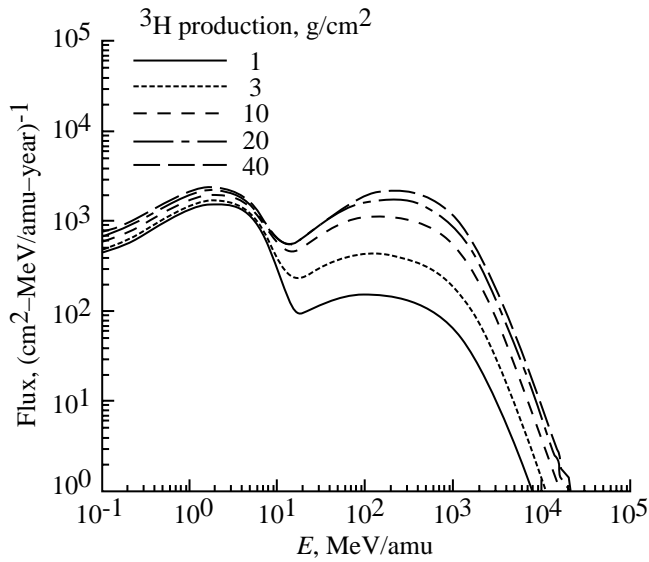
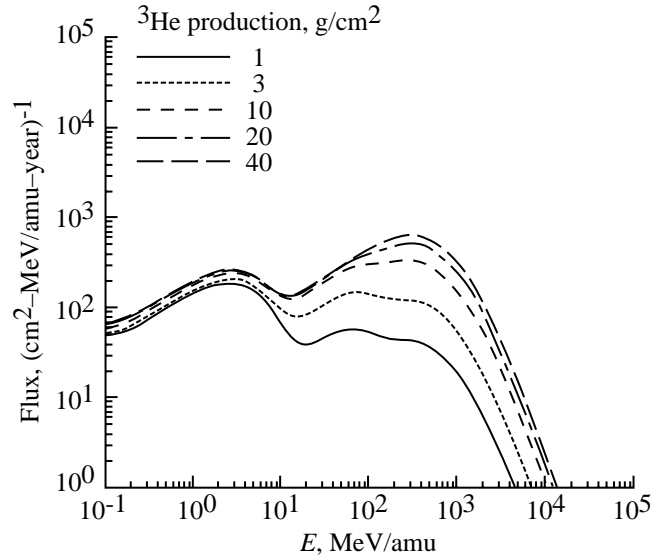
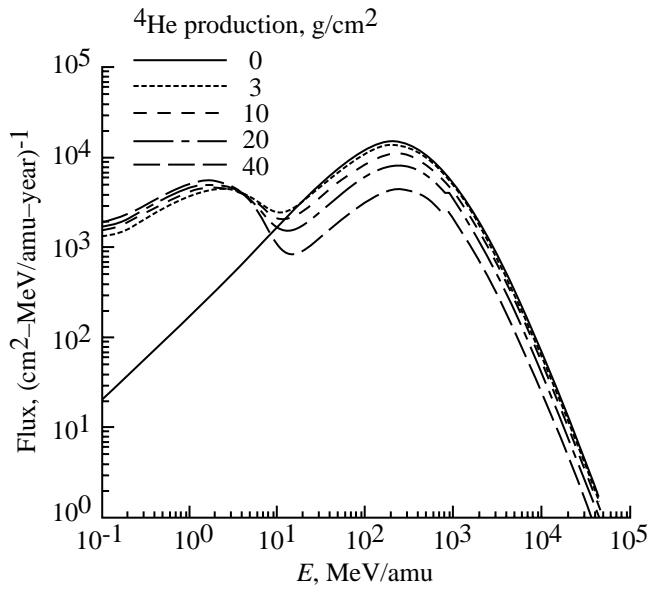


Figure 15. Calculations of light-ion flux spectrum in water shields.

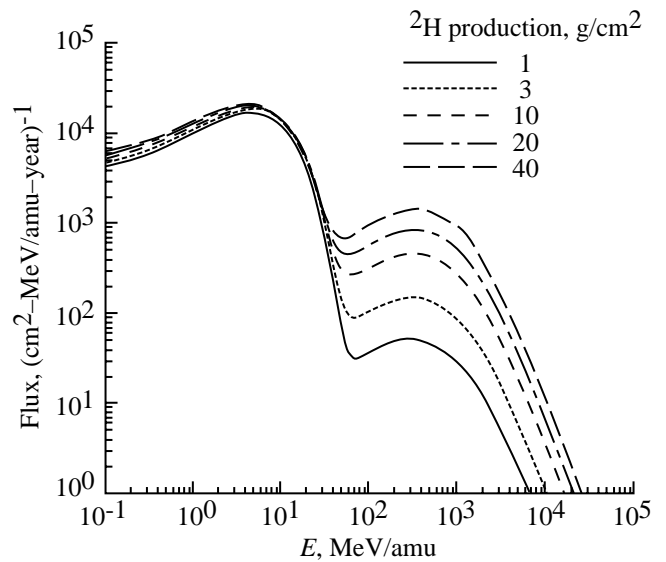
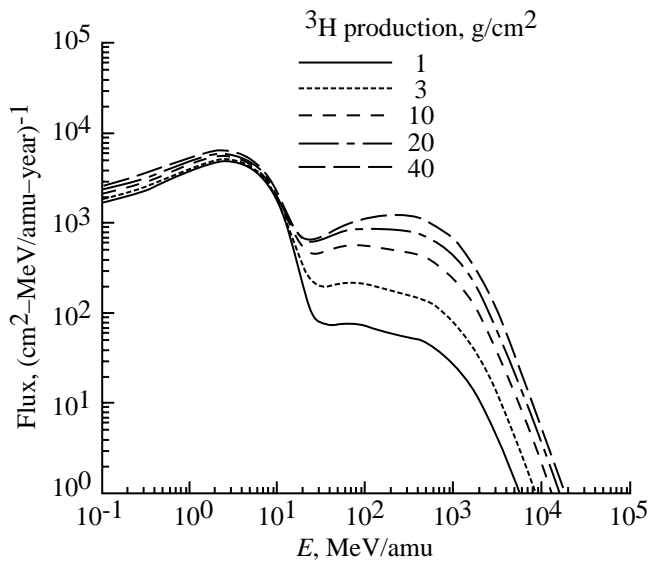
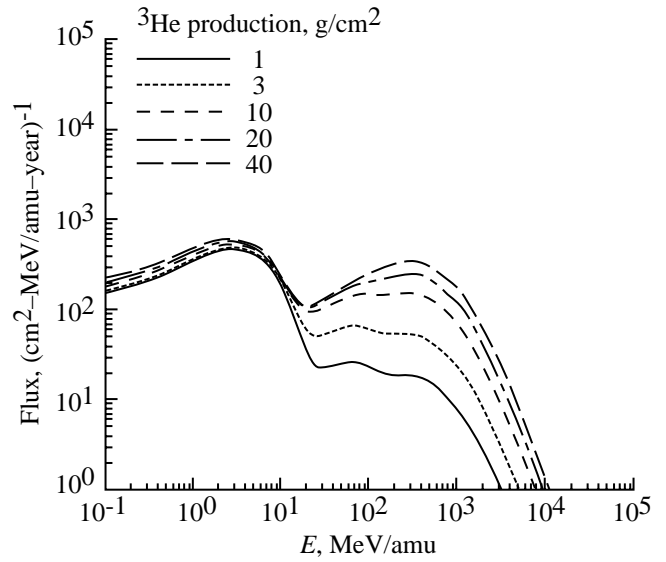
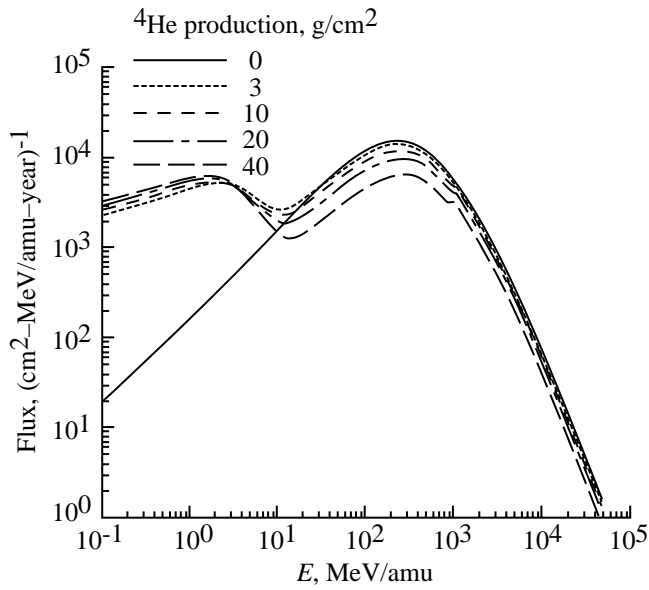
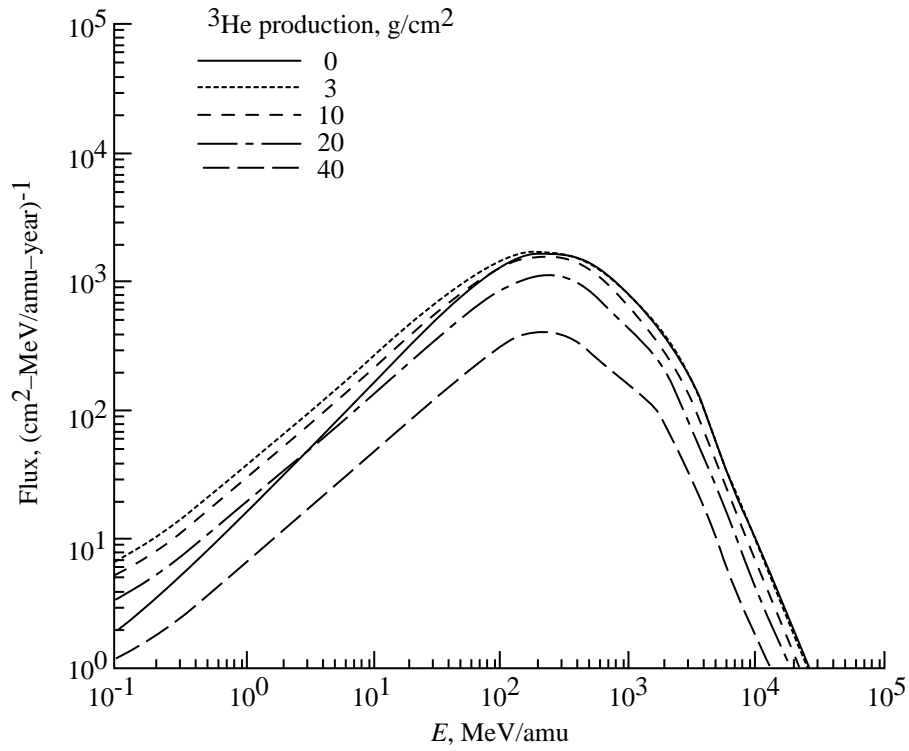
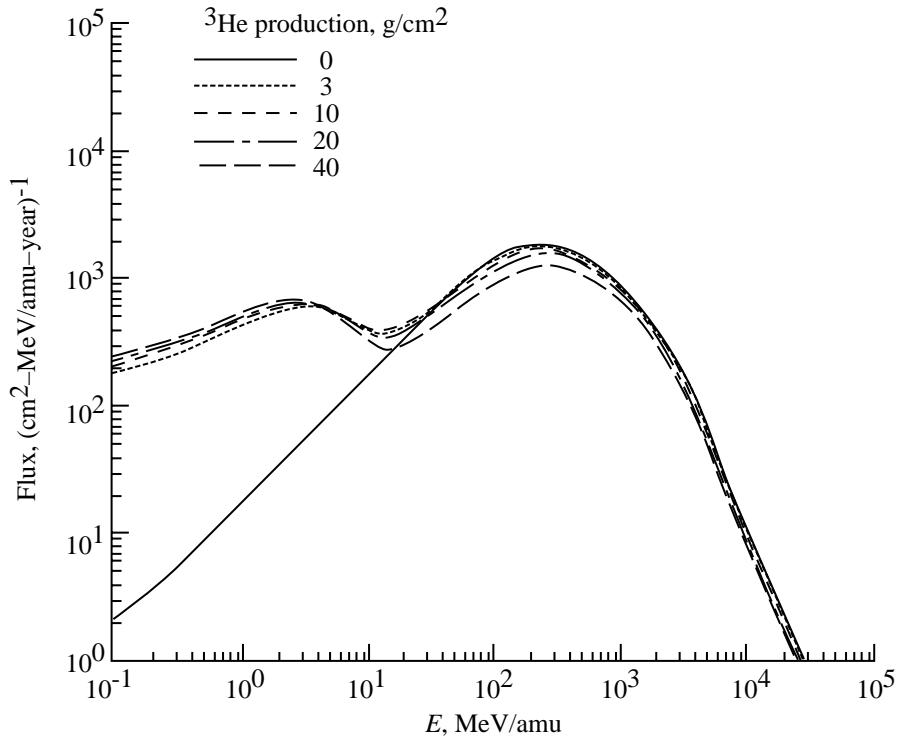


Figure 16. Calculations of light-ion flux spectrum in aluminum shields.



(a)  $^3\text{He}$  production for liquid hydrogen shield.



(b)  $^3\text{He}$  production for aluminum shield.

Figure 17. Calculations of flux spectrum of  $^3\text{He}$  in  $\text{H}_2$  and aluminum shields with primary component included.

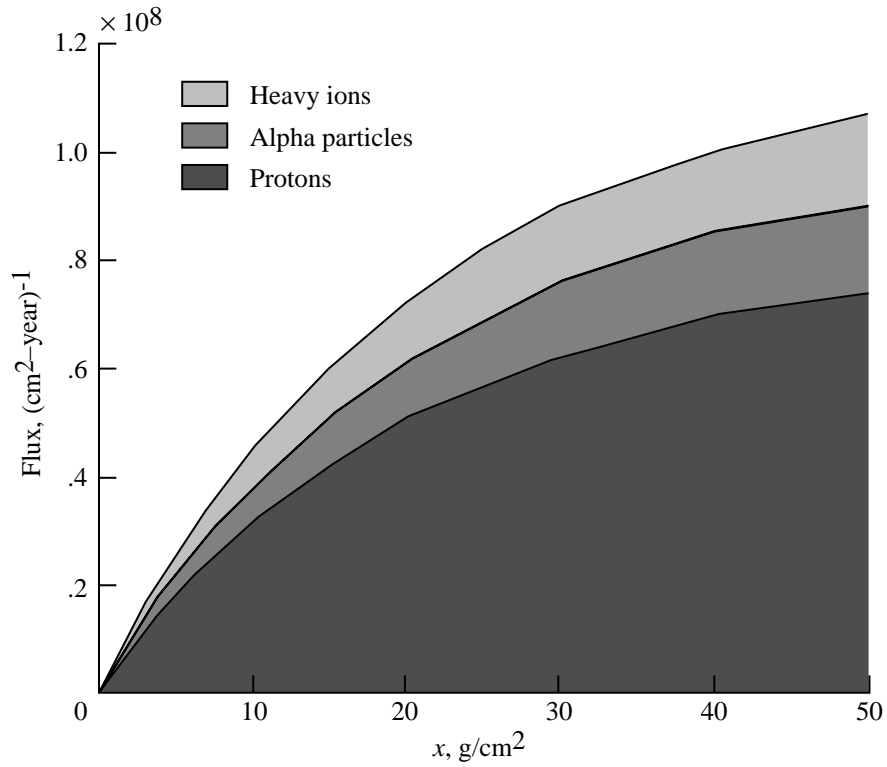


Figure 18. Secondary neutron flux contributed versus depth in water shield.

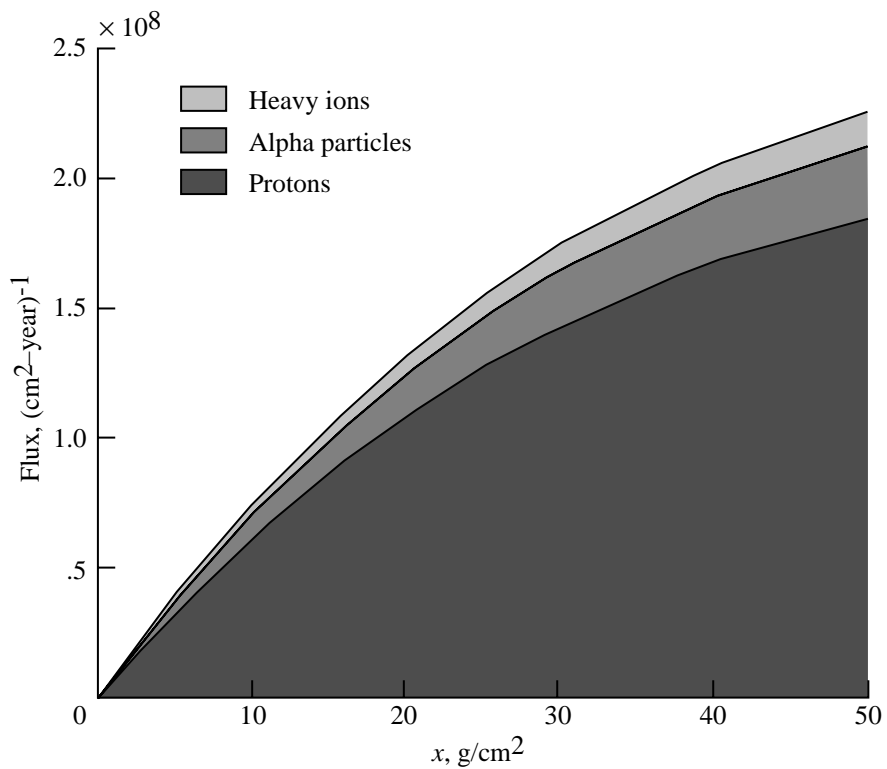


Figure 19. Secondary neutron flux contributed versus depth for aluminum shield.

REPORT DOCUMENTATION PAGE			Form Approved OMB No. 0704-0188	
Public reporting burden for this collection of information is estimated to average 1 hour per response, including the time for reviewing instructions, searching existing data sources, gathering and maintaining the data needed, and completing and reviewing the collection of information. Send comments regarding this burden estimate or any other aspect of this collection of information, including suggestions for reducing this burden, to Washington Headquarters Services, Directorate for Information Operations and Reports, 1215 Jefferson Davis Highway, Suite 1204, Arlington, VA 22202-4302, and to the Office of Management and Budget, Paperwork Reduction Project (0704-0188), Washington, DC 20503.				
1. AGENCY USE ONLY (Leave blank)	2. REPORT DATE November 1993	3. REPORT TYPE AND DATES COVERED Technical Paper		
4. TITLE AND SUBTITLE Calculations of Cosmic-Ray Helium Transport in Shielding Materials			5. FUNDING NUMBERS WU 199-45-16-11	
6. AUTHOR(S) Francis A. Cucinotta				
7. PERFORMING ORGANIZATION NAME(S) AND ADDRESS(ES) NASA Langley Research Center Hampton, VA 23681-0001			8. PERFORMING ORGANIZATION REPORT NUMBER L-17225	
9. SPONSORING/MONITORING AGENCY NAME(S) AND ADDRESS(ES) National Aeronautics and Space Administration Washington, DC 20546-0001			10. SPONSORING/MONITORING AGENCY REPORT NUMBER NASA TP-3354	
11. SUPPLEMENTARY NOTES				
12a. DISTRIBUTION/AVAILABILITY STATEMENT  Unclassified-Unlimited  Subject Category 93			12b. DISTRIBUTION CODE	
13. ABSTRACT (Maximum 200 words) The transport of galactic cosmic-ray helium nuclei and their secondaries through bulk shielding is considered using the straight-ahead approximation to the Boltzmann equation. A data base for nuclear interaction cross sections and secondary particle energy spectra for high-energy light-ion breakup is presented. The importance of the light ions $^2\text{H}$ , $^3\text{H}$ , and $^3\text{He}$ for cosmic-ray risk estimation is discussed, and the estimates of the fractional contribution to the neutron flux from helium interactions compared with other particle interactions are presented using a 1977 solar minimum cosmic-ray spectrum.				
14. SUBJECT TERMS Galactic cosmic rays; Alpha particles; Nuclear fragmentation; Radiation risk			15. NUMBER OF PAGES 33	
			16. PRICE CODE A03	
17. SECURITY CLASSIFICATION OF REPORT Unclassified	18. SECURITY CLASSIFICATION OF THIS PAGE Unclassified	19. SECURITY CLASSIFICATION OF ABSTRACT	20. LIMITATION OF ABSTRACT	